npj | materials sustainability

Review

https://doi.org/10.1038/s44296-025-00069-5

Lithium resources and novel strategies for their extraction and purification

Fangshuai Wu, Karthik R. Shivakumar, Kurt O. Konhauser & Daniel S. Alessi ✉

The demand for lithium (Li) for batteries has risen sharply. This review discusses Li resources (igneous rocks, clays, brines), production methods, and Li recycling from spent batteries. We highlight direct lithium extraction (DLE) techniques, focusing on lithium manganese oxides (LMOs). As challenges like sorbent degradation continue to be problematic, doping, surface coating, and the use of composites are explored as strategies to enhance LMO performance for sustainable Li production.

Lithium (Li) is a reactive alkali metal notable for its high electrochemical potential, low density, and high heat capacity. These properties make it indispensable in a range of industrial applications, including rechargeable batteries for electronic devices and electric vehicles (EVs), pharmaceuticals, ceramics, lubricants, and even nuclear fusion research[1,2]. Demand for Li has recently surged, driven largely by the rapid growth of the EV market and the increasing demand for portable electronic devices. The global shift towards clean energy and efforts to reduce carbon emissions have further accelerated the demand, as Li is essential for energy storage solutions for renewable technologies like solar and wind power. According to the United States Geological Survey (USGS), global Li consumption in 2024 was estimated at approximately 220,000 tons increased by 29% from 170,000 tons in 2023, with the battery industry accounting for 87% of this total[2]. Projections suggest that global demand for Li will surpass 2 million tons by 2030 and 5 million tons by 2050[3–5]. However, there are concerns that existing Li resources may be depleted by 2080[3].

Lithium resources are abundant globally, with major deposits located in Bolivia, Argentina, the United States, Chile, Australia, and China[2,6]. Despite this abundance, extracting and processing Li presents challenges, as these methods can have considerable environmental impacts. Furthermore, geopolitical considerations, market dynamics, and supply chain vulnerabilities highlight the need for diversifying Li resources and developing sustainable production practices[7,8]. Efforts are ongoing to expand Li production capacity, improve extraction efficiency, and explore alternative resources to ensure a stable and reliable supply of Li for future technological advancements.

This review offers a thorough examination of Li resources, detailing traditional extraction methods applied and their environmental impacts. It also explores advanced technologies, such as direct lithium extraction (DLE), which targets unconventional resources like low-concentration brines. Additionally, the review highlights recent advancements in ion-exchange type DLE materials, specifically lithium manganese oxides (LMOs), and discusses their potential as one of the most promising candidates for DLE applications.

Lithium resources

In 2024, the USGS estimated that the global identified Li resource to be approximately 115 million tons lithium carbonate equivalent (LCE)[2]. Bolivia and Argentina are the top holders, each accounting for 20.0% of global Li resources, followed by the United States (16.5%), Chile (9.6%), Australia (7.7%), and China (5.9%) (Fig. 1a)[2]. Lithium occurs naturally in various forms including igneous rocks, clays, brines, and seawater. Among these, igneous rocks and brines are the two largest resources, accounting for about 14% and 78% of the total, respectively[9]. These resources collectively constitute 25% and 65% of global production, respectively[10–12].

Global Li production in 2024 increased by 18% to 240,000 tons from 204,000 tons in 2023[2]. Australia remained the leading producer, contributing 88,000 tons (36.7%), followed by Chile with 49,000 tons (20.4%) and China with 41,000 tons (17.1%) (Fig. 1c)[2]. Emerging producers like Zimbabwe (22,000 tons, 9.2%) and Argentina (18,000 tons, 7.5%) made significant contributions, while Brazil contributed 10,000 tons (4.2%)[2]. Smaller contributions came from Canada (4,300 tons, 1.8%), Namibia (2,700 tons, 1.1%), and Portugal (380 tons, 0.2%)[2]. Note that the United States production data is withheld by the USGS to protect proprietary company information.

Lithium in igneous rocks

The most significant igneous Li deposits are found in granitic pegmatites[3,5,10,13–16]. Pegmatites are globally abundant, with most Li-bearing pegmatites located in Australia, China, the United States, and Canada[5,14,17]. Lithium concentrations in these rocks typically range between 1 and 4 wt%[13,14]. Within pegmatites, Li occurs in various mineral forms, including aluminosilicates minerals, such as spodumene ($LiAlSi_2O_6$), lepidolite ($KLi_{1.5}Al_{1.5}[Si_3O_{10}][F, OH]_2$), petalite ($LiAlSi_4O_{10}$), and zinnwaldite ($KLiFeAl[AlSi_3]O_{10}[OH,F]_2$) as well as and phosphate minerals like amblygonite ($LiAl[PO_4][OH, F]$)[3,10,13,14,18]. Among these minerals, spodumene is the most commercially important for large-scale production due to its high Li content (1.9–3.7 wt%), abundance, and ease of commercial processing[3,13,19]. Australia is currently the largest producer of Li from spodumene[19,20]. Petalite, which can contain 1.4–2.2 wt% Li[19], is used mainly

Department of Earth and Atmospheric Sciences, University of Alberta, Edmonton, AB, Canada. ✉e-mail: alessi@ualberta.ca

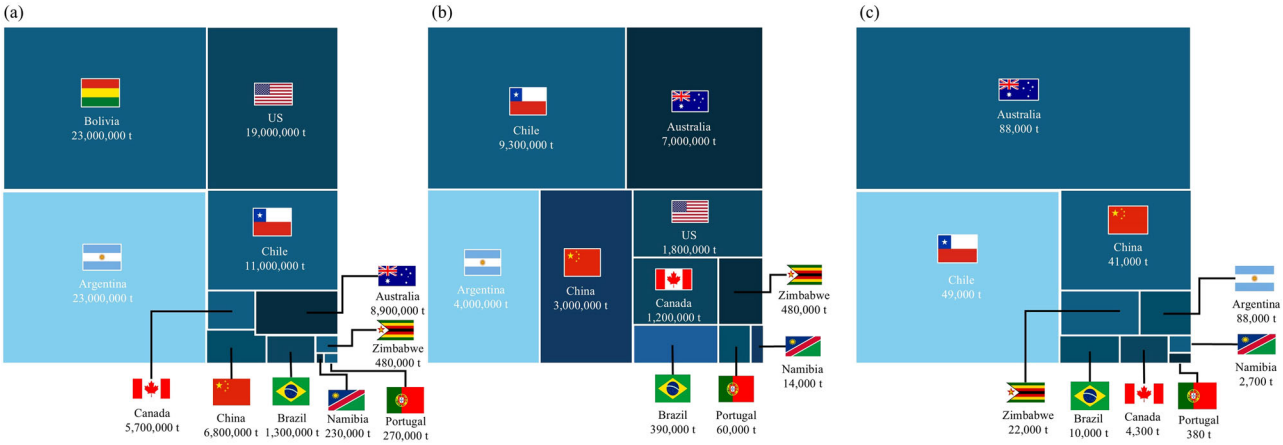

Fig. 1 | Global lithium distribution and production in 2024. Estimated **a** Li resources, **b** Li reserves, and **c** Li production in 2024 by country[2].

in glass, glazes, and ceramics due to its low thermal expansion properties[3]. Large petalite deposits occur in southern Zimbabwe, Namibia, Brazil, and Australia[19,21]. While lepidolite, with a Li content of 1.4–3.6 wt%[19], was once mined for Li, it is no longer favored due to its elevated fluorine (F) content, which can release potentially hazardous volatile compounds during processing[3].

Lithium in clays

Lithium-bearing clays are recognized as potential Li resources, primarily found in Mexico, the United States, and Serbia[10]. Currently, Li-bearing clays represent the third largest Li resources globally, contributing approximately 10% of total production[10]. The primary Li-bearing clays include hectorite ($Na_{0.33}[Mg,Li]_3Si_4O_{10}[F,OH]_2$) and jadarite ($LiNaSiB_3O_7(OH)$)[9,19]. Hectorite typically contains Li concentrations ranging from 0.3 to 0.6 wt%[19], while jadarite has a Li content of approximately 0.8 wt%[22,23]. Historically, these Li-bearing clays were not considered economically viable for Li production, but rising demand has led to increased interest in developing these resources[24].

Lithium in brines

Lithium in brines is typically in its ionic form, specifically as the lithium ion (Li^+). Brines, which host approximately 78% of global Li resources[9] can be classified into three types: continental, geothermal, or oilfield. Among these, continental brines account for 59% of global Li production[10–12]. Continental brines, also referred to as salt lakes or salar brines, are recognized for their high Li contents, typically ranging from 54 to 1600 $mg{\cdot}L^{-1}$, with some reaching nearly 5000 $mg{\cdot}L^{-1}$[13,25]. These brines are predominantly located in the salt lakes of Argentina, Bolivia and Chile, collectively referred to as the "Lithium Triangle"[26]. In contrast, salt lakes in the US and China have lower Li concentrations (typically <500 $mg{\cdot}L^{-1}$)[25].

Many countries also possess geothermal and oilfield brines, or access to seawater, as potential Li sources. Geothermal and oilfield brines, which are byproducts of geothermal energy production and oil and gas extraction, typically host Li concentrations that vary from negligible to over 400 $mg{\cdot}L^{-1}$, though most lie between 0.5 and 37 $mg{\cdot}L^{-1}$[25]. Seawater, while a vast potential Li resource, has a much lower concentration of about 0.17 $mg{\cdot}L^{-1}$[25]. For seawater to become an economically viable source of Li, it requires processing to concentrate the Li content. Existing Li extraction processes from low Li-bearing brines like seawater and geothermal brines typically becomes viable only when concentrations exceed 75 $mg{\cdot}L^{-1}$[27]. However, the presence of dissolved organic compounds and hydrogen sulfide (H_2S) in the brines require an even higher Li concentration for the process to remain economically feasible[28], as additional pretreating expenses need to be accounted for. Additionally, these Li-bearing brines normally contain high concentrations of impurities, such as sodium (Na^+), magnesium (Mg^{2+}), calcium (Ca^{2+}), potassium (K^+), strontium (Sr^{2+}), and borate ($B(OH)_4^-$) which can complicate and reduce the efficiency of Li recovery[1,29–31].

Lithium in batteries

Lithium-ion batteries (LIBs) are electrochemical devices that store and release energy through the movement of lithium ions between the anode and the cathode. LIBs are extensively used in consumer electronics, including smartphones, laptops, and tablets, as well as in EVs, due to their high energy density, long cycle life, and reliability. Their performance has made them essential in powering modern portable devices and enabling transportation to begin to transition to EVs.

LIBs contain several key components, each critical to its performance, safety, and longevity. These include the cathode, anode, electrolyte, separator, current collectors, and battery casing. The cathode, typically made from lithium metal oxides such as lithium cobalt oxide ($LiCoO_2$ or LCO), lithium manganese oxide ($LiMn_2O_4$ or LMO), lithium nickel manganese cobalt oxide ($LiNiMnCoO_2$ or NMC) or lithium iron phosphate ($LiFePO_4$ or LFP), is the source of lithium ions. The anode, usually made of graphite, allows for the intercalation of lithium ions during charging. The electrolyte, often a Li salt (e.g., $LiPF_6$, $LiClO_4$ and $LiBF_4$) dissolved in an organic solvent, permits the movement of lithium ions between the cathode and anode during charging and discharging cycles. A porous separator prevents physical contact between the electrodes while allowing ion flow, ensuring safe operation. Current collectors, typically aluminum for the cathode and copper for the anode, facilitate electron transfer between the electrodes and the external circuit. The battery casing, made from metal or laminated composites, provides structural integrity, prevents leaks, and protects internal components from environmental damage. LIBs contain 2–7 wt% of Li, a concentration significantly higher than that found in natural ores[1]. This high Li content makes spent LIBs an important secondary resource for Li recovery, and a sustainable potential alternative to traditional Li production from igneous rocks and brines.

The rapid adoption of EVs has increased demand for LIBs. In 2021, global EV sales were 6.6 million units, a threefold increase compared to 2019[32]. Projections indicate that by 2040, EVs will account for 58% of all vehicles sold worldwide[33]. In 2019, approximately 5.6 million EVs were in use globally[33], and this number is projected to rise to around 10 million by 2025[1]. Every year, an increasing number of electric vehicles reach their end-of-life, as LIBs in these vehicles are typically used for 5–8 years or until their capacity declines to 70–80% of the original capacity, leading to the generation of a substantial volume of spent batteries[34]. However, only 32% of LIBs are currently recycled[35]. The International Energy Agency estimates that end-of-life EVs in 2019 generated 500,000 tons of LIB waste, and the total amount of waste generated by 2040 could be as much as 8 million tons[33]. It is estimated that the recycling of approximately 28 tons of LIBs from smartphones and laptops, or 256 EV batteries, can yield 1 ton of LCE[36].

Thus, recycling spent LIBs as a secondary resource for Li recovery could yield over 280,000 tons LCE per year by 2040, which would substantially reduce dependence on further Li mining.

Latest lithium deposit discoveries

Over the past five years, substantial Li deposits have been discovered worldwide. According to the USGS, global identified Li reserves have increased by nearly 43% since 2019, reaching approximately 30 million tons as of 2024[2]. One of the most significant trends is the exploration of non-traditional Li sources. Traditionally, Li has been extracted from igneous-rock mining or brine deposits in salt flats. However, countries are increasingly exploring unconventional sources such as oilfield and geothermal brines. For instance, in the United States, Li extraction from oilfield brines in the Smackover Formation in Arkansas is gaining traction, with high Li concentrations (>400 ppm) observed in some of these brines[37]. This approach represents an opportunity to extract Li from what is otherwise a waste stream. Similarly, projects in California, Russia, Philippines, China, and Indonesia are exploring the potential of geothermal brines[14].

In the United States, discoveries have been made in Arkansas and Nevada. The Smackover Formation in southwestern Arkansas, estimated by the USGS in October 2024 to contain between 5 and 19 million tons of Li[37], has the potential to meet global Li demand for electric vehicle batteries up to nine times over by 2030. Nevada's Thacker Pass Li mine, the largest known Li deposit in the United States, has been under development since 2007. Estimates suggest this deposit contains between 20 to 40 million tons of Li[38]. Construction began in March 2023, and the mine is expected to achieve a total nominal design capacity of 160,000 tons per year of battery-quality lithium carbonate (Li_2CO_3) by 2039[39]. A major Li deposit in the Reasi District of Jammu and Kashmir was also discovered in India in 2022. The Geological Survey of India (GSI) announced that the region holds approximately 5.9 million tons of Li ore[35]. Australia will continue to be a key contributor to global Li supply. For example, the Finniss Lithium mine in the Northern Territory of Australia, discovered in 2016, began commercial production in February 2023, with an estimated resource of 48.2 million tons at 1.26% lithium oxide as of September 2024[40]. The Canadian Li exploration company E3 Lithium estimated that the Bashaw District in Alberta, Canada hosts 3.05 million tons of Li within the Nisku and Leduc aquifers[41].

The exploration and development of Li resources is underway globally, reflecting the strategic importance of securing supply chains to meet rapidly increasing demand. According to the USGS, as of 2024, brine-based Li deposits are currently under exploration or development in several countries, including Argentina, Bolivia, Canada, Chile, China, and the United States[2]. Meanwhile, mineral-based Li resources are being explored or developed in places including Australia, Austria, Brazil, Canada, China, Congo (Kinshasa), Czechia, Ethiopia, Finland, France, Germany, Ghana, India, Iran, Kazakhstan, Mali, Namibia, Nigeria, Peru, Portugal, Russia, Rwanda, Serbia, Spain, Thailand, Turkey, the United States, and Zimbabwe[2]. Furthermore, Li-clay deposits are under investigation or development in Mexico and the United States[2]. This widespread activity indicates a global effort to diversify and identify new Li sources.

Lithium production

Commercial Li production from rocks and brines primarily involves two methods: leaching and solar evaporation. These processes yield two major Li end-products, Li_2CO_3 and lithium hydroxide (LiOH), both of which are widely used in battery manufacturing, ceramics, and pharmaceuticals. In addition to Li extraction from rocks and brines, there is increasing interest in the recovery of Li from spent batteries. A comprehensive overview of the methodologies employed in the extraction and processing of Li from hard rock mining, brines, and spent batteries is presented below and summarized in Table 1. Note that capital expenditures (CAPEX) are excluded from Table 1, as its value varies significantly depending on the scale and scope of the mining operation.

Table 1 | Comparison of Li extraction methods: igneous rock mining, brine (solar evaporation), brine (DLE), and recycling (spent batteries)

	Igneous Rock Mining	Brine (Solar Evaporation)	Brine (DLE)	Recycling (Spent Batteries)
Production Duration	Weeks to months	Months to years	Hours to days	Days to weeks
Li Recovery Rates	~60–80%	~40–60%	~75–99.99%	Up to 90%
Li Product	Spodumene concentrate (requires conversion to Li_2CO_3 or LiOH)	Li_2CO_3 or LiCl	Li_2CO_3 or LiOH	Li_2CO_3 or LiOH or various cathode materials
Cost	Medium to High	Low to Medium	Low to Medium	Medium
OPEX	3600–8000 USD/t LCE	$3300–4,900 USD/t LCE	$2800–4600 USD/t LCE	~$2250 USD/t LIB
Pre-treatment Requirements	Crushing, grinding, flotation	Minimal, requires brine with high Li concentration	Requires brine or geothermal fluids, some chemical adjustments	Battery collection, sorting, discharge
Post-treatment Requirements	Roasting, sulfuric acid leaching, purification	Carbonate precipitation, chemical purification	Lithium precipitation, solvent extraction, further purification	Mechanical/chemical processing, hydrometallurgical or pyrometallurgical refining
Weather Dependence	Low (operations run year-round)	High (evaporation rate depends on temperature, humidity, and wind)	Low (can operate in any climate)	Low (indoor facilities)
Land Requirements and Impacts	High (Large mines, tailings, significant land disturbance)	High (Large evaporation ponds, long-term land use)	Low (Minimal land impact, mostly occurs at existing facilities)	Low (processing plants in industrial zones)
Water Consumption	High (ore processing, dust suppression, and chemical leaching)	High (large water losses due to evaporation)	Low (water can often be recycled)	Low to moderate (depends on method)
Energy Consumption	High (mining, crushing, roasting)	Low (mostly passive evaporation, pumping, chemical processing)	Moderate to high (pumping, chemical processing)	Moderate (chemical extraction requires energy)
Green House Gas Emissions	High (due to fossil fuel use in mining and processing)	Low (mainly from brine pumping)	Low to moderate (depends on energy source/ DLE type)	Low to moderate (avoids mining emissions)

Source: The Goldman Sachs Group, Inc[43]., Ibarra-Gutierrez et al.[44]., Boroumand and Razmjou[45]., and Dalini et al.[36].

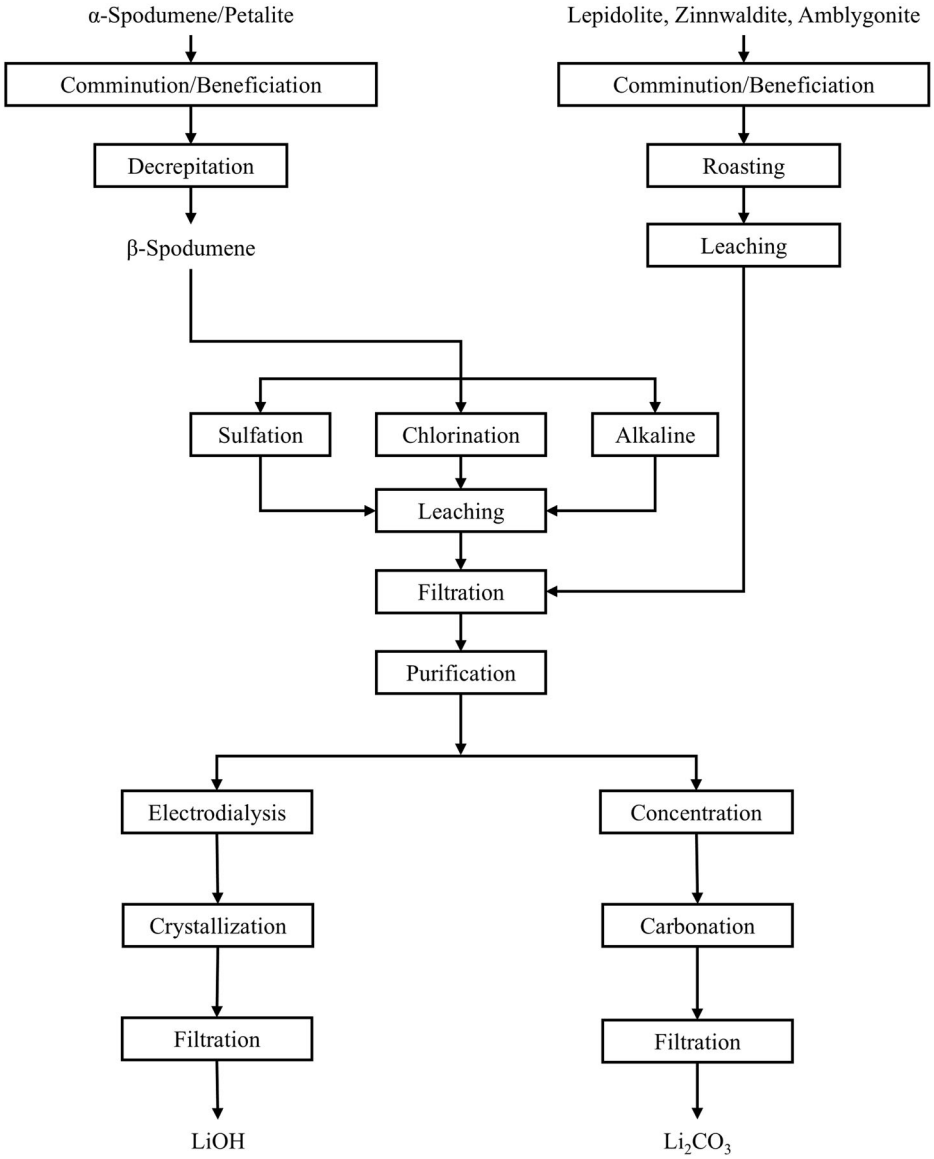

Fig. 2 | Flow diagram of Li production from igneous rocks. Adapted from Tran and Luong[13] and Meng et al.[1].

Lithium production from igneous rocks

Lithium production from igneous rocks contributes approximately 25% of global Li production[10–12]. Spodumene is the dominant Li-bearing mineral, accounting for around 90% of Li production from non-brine sources worldwide[1]. The initial processing phase involves crushing and grinding the spodumene (as shown in Fig. 2), followed by flotation to increase its concentration. This process yields a concentrate containing approximately 6 wt % Li_2O[13]. The concentrate is then treated in a rotary kiln at temperatures ranging from 1040 to 1100 °C to convert α-spodumene to β-spodumene[1], as β-spodumene is a more readily extractable form of Li for chemical processing. Subsequently, β-spodumene undergoes one of three roasting processes: sulfation, chlorination, or alkaline treatment. In the sulfation method, β-spodumene is converted into soluble lithium sulfate (Li_2SO_4) by baking it with concentrated sulfuric acid (H_2SO_4) at 250 °C[13]. The chlorination method involves roasting β-spodumene with various chlorinating agents such as hydrochloric acid (HCl), calcium chloride ($CaCl_2$), sodium chloride (NaCl), or chlorine gas (Cl_2) at temperatures ranging from 800 to 1100 °C, resulting in the formation of soluble lithium chloride (LiCl)[1]. Lastly, alkaline treatment uses calcite ($CaCO_3$) or soda ash (Na_2CO_3) at temperatures between 825 and 1050 °C to produce soluble lithium oxide (Li_2O)[42].

The process for other Li-bearing ores such as lepidolite, zinnwaldite, and amblygonite closely resembles that of spodumene in the initial stages. However, it involves a simpler one-step roasting process with additives such as calcium sulfate ($CaSO_4$), calcium oxide (CaO), and $CaCO_3$, at temperatures ranging from 800 to 1000 °C, followed by water leaching[1]. During the purification process, impurities, such as Na^+, Mg^{2+}, Ca^{2+}, K^+, aluminum (Al^{3+}), and iron (Fe^{2+}) are removed through precipitation. The resulting raw Li compounds can then be converted into LiOH or Li_2CO_3 by reacting to them with sodium hydroxide (NaOH), carbon dioxide (CO_2), or Na_2CO_3, depending on the desired final products.

Lithium extraction from hard rock deposits presents significant economic and environmental challenges. The process requires weeks to months to complete and is associated with a high operational expenditure (OPEX) ranging from $3600 to $8000 USD per ton of LCE[43,44]. These costs are driven by the intensive mechanical and chemical processing required, including crushing, grinding, flotation, and high-temperature roasting. The environmental impacts of hard rock mining are equally concerning. The method necessitates extensive land disturbance, with an average of 335 m^2 of direct land use per ton of LCE, primarily due to open-pit mining and the construction of tailings dams[45]. This leads to habitat destruction, soil erosion, and the potential contamination of surface and groundwater systems[46]. The leaching of processing reagents, such as H_2SO_4 and NaOH, along with heavy metals and other naturally occurring contaminants, has been documented. For example, studies on the proposed Li extraction site in Serbia's Jadar

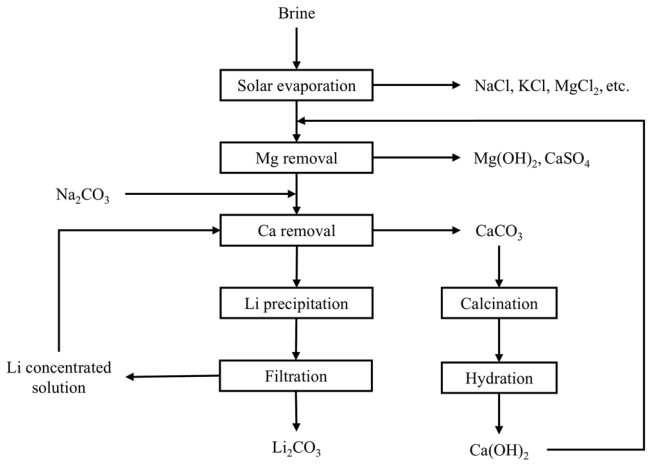

Fig. 3 | Flow diagram of Li production from continental brines. Adapted from Tran and Luong[13] and Meng et al.[1].

Valley revealed elevated concentrations of boron, arsenic, and lithium in downstream river areas[47]. Furthermore, the disposal of tailings and wastewater poses additional environmental risks if not managed properly.

In addition to land-use impacts, hard rock Li mining is resource-intensive, particularly in terms of water and energy consumption. The process requires approximately 161 m^3 of water per ton of LCE, used primarily for ore processing, dust suppression, and chemical leaching[45]. Energy demands are also high, driven by the high-temperature roasting and refining stages, which are usually powered through the combustion of coal and other fossil fuels. This results in substantial greenhouse gas (GHG) emissions, estimated at 58.4 tons of CO_{2eq} per ton of LCE[45]. These emissions are generated both from the direct combustion of fossil fuels and the energy-intensive nature of the subsequent concentration and refining steps. Developing greener extraction technologies are essential to improve sustainability, reduce reagent/energy consumption, and minimize the environmental impacts of Li ore processing.

Lithium production from continental brines

Currently, most global production of Li production comes from continental brines. For decades, the primary method for extracting Li from these brines has combined solar evaporation with precipitation. This approach stands as the sole method employed in large-scale industrial Li from continental brines owing to its simplicity and cost-effectiveness. The OPEX for solar evaporation ranges from 3300 to 4,900 USD per ton of LCE[43]. This economic efficiency is primarily driven by its reliance on solar energy, which reduces Li extraction costs from brines by 30–50% compared to extraction from igneous rocks[1]. However, because solar energy is required, this method is geographically limited to regions with long summer days, moderate wind, little rain, and low humidity, which promote water evaporation[48]. Due to these geographic limitations, there are only eight large-scale commercial facilities currently employing this method worldwide. These include two in Argentina (Salar de Olaroz and Salar de Hombre Muerto), two in Chile (at the Salar de Atacama), three in China (Dontai Salt Lake, Xintai Salt Lake, and Lake Zabuye), and one in the USA (Clayton Valley)[49].

Due to variations in aqueous chemistry amongst different continental brines, the Li production process varies. A general flow diagram of this process is depicted in Fig. 3 to illustrate its key stages and components. In the initial stage, Li-bearing brine is extracted from underground reservoirs or salt lakes and subsequently pumped into large evaporation ponds. During this process, salts begin to precipitate in the order of their solubility: halite (NaCl), sylvite (KCl), sylvinite (NaCl·KCl), magnesium salts (e.g., $MgCl_2$) and other alkali salts[1]. Over several months of solar evaporation, the brine concentration increases may reach approximately 6000 mg·L^{-1}[50]. Depending on the initial Li concentration in the brine, anywhere from 30% to more than 90% of the water evaporates throughout this extended process. The remaining concentrated brines are then transferred to recovery ponds where they undergo treatment with lime ($Ca(OH)_2$). This treatment aims to remove dissolved magnesium (Mg) and sulfate (SO_4^{2-}), precipitating them as magnesium hydroxide ($Mg(OH)_2$) and $CaSO_4$, respectively. Subsequently, sodium carbonate (Na_2CO_3) is added to remove Ca^{2+} as calcium carbonate ($CaCO_3$). Later in the precipitation process, Li_2CO_3 begins to precipitate after further addition of Na_2CO_3. This initial Li_2CO_3 product typically goes through repeated dissolution and re-precipitation processes to reach battery-grade purity (>99.5 wt%)[3].

The concentration of Mg^{2+} in brines plays an important role in the evaporation and precipitation process for Li extraction. Initially, elevated levels of Mg^{2+} can slow evaporation and inhibit the formation of the solid LiCl. Moreover, excess Mg^{2+} leads to overconsumption of the precipitants $Ca(OH)_2$ and Na_2CO_3, resulting in a higher processing cost and the loss of Li. For these reasons, brines with Mg/Li mass ratios exceeding 10 are not economically feasible using conventional evaporation and precipitation methods[3]. Despite its cost advantages, the solar evaporation method is time-consuming, as well as water- and land-intensive. Depending on climatic factors, such as sunlight, humidity, and rainfall, the Li extraction process can take between 12 and 24 months[49]. Additionally, substantial volumes of water, ranging from 100 to 800 m^3 per ton of Li_2CO_3, are lost during the process[49]. Meanwhile, fresh groundwater from neighboring areas is often drawn into the production field or salt lakes, where it is mixed with brine[49]. Once mixed, it is no longer considered fresh and is unsuitable for human consumption or agricultural purposes. Additionally, large evaporation ponds require substantial land use, encompassing areas for the ponds themselves, processing facilities, wellfields, and disposal zones. In major production sites such as Salar de Atacama and Salar de Cauchari, direct land usage ranges from 2949 to 3656 m^2 per ton of LCE[45]. More importantly, this traditional process only achieves a ~50% Li recovery rate in brines with low Mg/Li ratios, such as those found in South America, with even lower recovery rates observed in brines with higher Mg/Li ratios[51]. This process can also lead to environmental and social concerns, as dissolved salts like Na_2CO_3 and Li_2CO_3 can leach into and contaminate soil and freshwater used by local communities.

Lithium recycled from spent batteries

Recycling Li from spent batteries is a critical process in reducing environmental impacts and ensuring a sustainable supply of Li for future battery production. Currently, there are more than 21 operational and 11 planned LIB recycling facilities, with a combined capacity exceeding 300,000 tons, located in East Asia, Europe, and North America[33]. The recycling process typically involves several steps, including collection, sorting, discharging, dismantling, and material recovery (Fig. 4). Current end-of-life battery recycling technologies include pyrometallurgical, hydrometallurgical and direct recycling approaches. The choice of optimal recycling methods depends on the type of lithium-ion battery. For instance, hydrometallurgical methods are more suitable for recycling NCM due to the necessity of separating multiple metals, whereas pyrometallurgical methods offer a simpler and more efficient approach for recycling LMO and LFP[33]. Direct recycling requires LIBs to be in good condition.

The process of recycling begins with the collection and sorting of spent batteries. Batteries are gathered from various sources, such as electronic waste recycling centers, automotive recycling facilities, and consumer drop-off points. They are then sorted by chemistry (e.g., lithium-ion, lithium-polymer) and type (e.g., cylindrical, prismatic, pouch). This sorting ensures that the recycling process is tailored to the specific battery chemistry, which improves efficiency and recovery rates. Once sorted, the batteries are discharged and handled safely to eliminate residual energy and reduce the risk of fire or explosion during processing. After discharge, the batteries undergo dismantling and mechanical processing. They are disassembled to separate components such as the casing, electrodes, and electrolyte. The battery cells are then shredded into smaller pieces to expose the internal materials. Mechanical processes like sieving, magnetic separation, and air classification

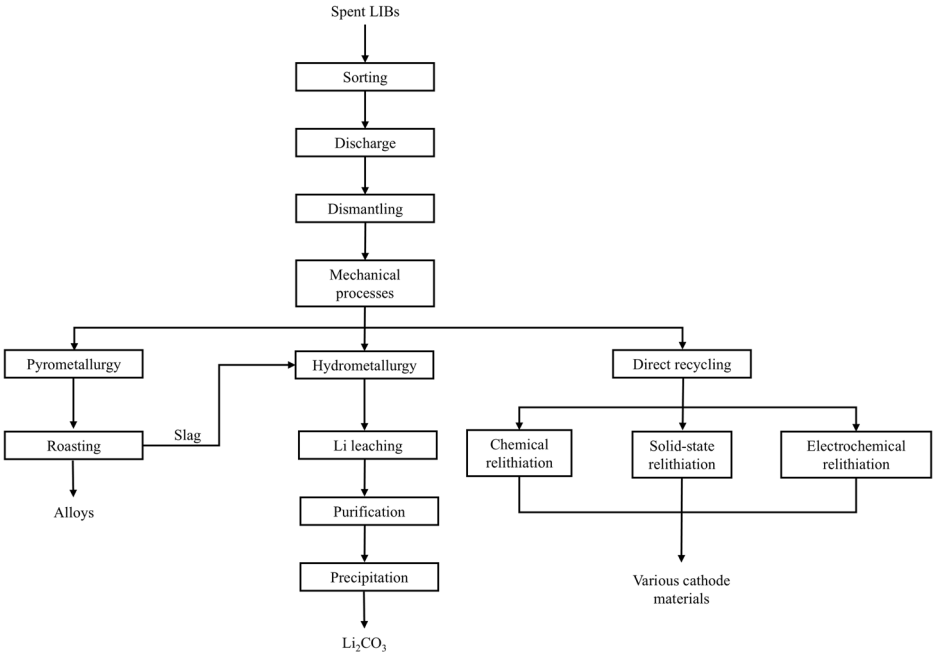

Fig. 4 | Flow diagram of Li production from spent batteries.

are used to separate metals (e.g., aluminum, copper, and steel) from the black mass, which is a mixture of cathode and anode materials containing lithium, cobalt, nickel, and graphite.

The next step is the hydrometallurgical process, which is one of the most common methods for Li recovery. The black mass is treated with acidic solutions (e.g., H_2O_2 with sulfuric acid or hydrochloric acid) to dissolve the metals, including lithium, cobalt, nickel, and manganese[33]. Impurities are removed through filtration, precipitation, or solvent extraction. Lithium is then recovered from the solution using methods such as precipitation (forming lithium carbonate or lithium phosphate), solvent extraction, electrochemical recovery, or crystallization. Alternatively, the pyrometallurgical process involves smelting the black mass or whole batteries in a furnace at high temperatures (above 1400 °C) to melt and separate metals[52]. During this process, organic materials such as electrolytes, separators, and binders are combusted, while metals are melted and separated. Following smelting, the molten materials settle into two distinct phases: a dense molten alloy and a lighter slag layer. The molten alloy, composed of valuable metals such as cobalt, nickel, and copper, accumulates at the bottom of the furnace due to its higher density. This alloy is tapped off and transferred to refining processes, where individual metals are isolated and purified for reuse in battery production or other industrial applications. The slag, a lighter layer of molten material floats on top of the metal alloy, contains lithium, aluminum, and other oxides. After the smelting process, the slag is cooled and solidified, then crushed into smaller pieces to facilitate further processing. Lithium recovery from slag is challenging due to its low concentration and the complex chemical composition of the slag. To extract Li, additional hydrometallurgical methods are typically required.

An emerging method is direct recycling, which focuses on recovering and reusing the cathode material directly without breaking it down into individual elements. A key step in direct recycling is relithiation, which restores the Li content of the cathode material that is often depleted during battery use. Relithiation can be achieved through several methods, including solid-state reactions, electrochemical processes, or chemical treatments. In solid-state relithiation, the cathode material is mixed with a Li source, such as Li_2CO_3, Li_3PO_4, or LiOH, and heated to temperatures between 600–800 °C[53]. This allows lithium ions to diffuse back into the cathode structure, replenishing its Li content. Electrochemical relithiation involves using the recovered cathode material as an electrode in an electrochemical cell, where lithium ions are re-inserted into the cathode structure through an applied voltage. Alternatively, chemical relithiation involves treating the cathode material with a Li-containing solution to restore its Li content. Direct recycling is particularly suited for spent LIBs whose active materials remain relatively intact and is applicable to most electrode chemistries, provided the electrode compositions are known[53]. Direct recycling has advantages that include reduced energy consumption and lower processing costs, as it preserves the structure of the cathode material. However, its implementation on a large scale requires precise sorting and processing to maintain material quality, presenting a challenge to widespread adoption.

The recycling of LIBs presents both environmental benefits and costs. Li et al. estimated that recycling 1 kg of LIBs generates GHG emissions ranging from 0.158 to 44.59 kg CO_2eq and requires energy inputs between 3.3 and 154.4 MJ[34]. LIBs recycling also has environmental costs, including transportation, the use of chemical reagents, and high energy use. Despite these challenges, recycling has a lower overall environmental footprint compared to traditional Li production. For example, by bypassing the carbon- and energy-intensive stages of mining and processing, recycling can significantly reduce GHG emissions. Specifically, LIB remanufacturing using materials recycled via pyrometallurgical, hydrometallurgical, and direct recycling methods has been shown to lower GHG emissions by 2.85%, 10.24%, and 34.52%, respectively[54], compared with manufacturing LIBs with virgin materials[54]. Furthermore, recycling can reduce energy consumption during material production by up to 48%[55].

Direct lithium extraction (DLE) from brines

To overcome the environmental, economic, and technical limitations of traditional evaporative methods, direct Li extraction (DLE) technologies are being explored as an alternative for recovering Li from brines. DLE offers significant advantages over traditional methods, including markedly shorter production durations (hours to days compared to months to years for solar evaporation), higher Li recovery rates (75–99.99%), and reduced land and water requirements due to its minimal land impact and ability to operate in any climate[43]. By eliminating the need for large, open-air evaporation ponds, DLE substantially minimizes the environmental footprint of Li recovery. Although DLE exhibits higher energy consumption compared to solar evaporation, its independence from weather conditions and potential for water recycling position it as a promising and sustainable alternative for Li extraction.

DLE is particularly promising for low Li-bearing brines, such as geothermal and oilfield brines, which are characterized by low Li^+ concentrations and high Mg/Li ratios. The economic feasibility of DLE depends on

several factors, including (1) the concentration of Li^+ in the brine, (2) ratio of competing ions to Li^+ (e.g., Mg/Li) in the brine, (3) the cost of materials and operation associated with DLE, (4) the duration of the production cycle, and (5) market demand and Li prices. Research has shown that solvent extraction, membrane, electrochemistry, adsorption, and ion exchange technologies are commonly utilized DLE methods for Li recovery from brine. Of these, adsorption is the only method currently used in commercial Li production[56], while the others remain in the development stage. A comprehensive overview of the DLE methods is presented below and summarized in Table 2.

Solvent extraction. Solvent extraction (Fig. 5a) of Li, also known as liquid-liquid extraction (LLE), is based on differences in the solubility of Li^+ in two immiscible liquid phases: an organic phase and an aqueous phase[3]. In this process, Li^+ from the brine (the aqueous phase) is transferred into the organic solvent (the organic phase) when the two are mixed. Subsequently, the Li^+ loaded organic phase is added to a recovery solution, typically an acid, where Li^+ is released. After Li^+ is stripped from the organic phase, the solvent can readily be reused in the next extraction cycle.

The effectiveness of solvent extraction depends heavily on the selection of appropriate extractants, which must be tailored to the specific chemistry of the brine. Three classes of extractants have been extensively studied: chelating, acidic, and ionic liquid extractants[3]. Studies have shown that combining acidic and neutral extractants can often yield the best separation and extraction results[3,57]. For example, a combination of acidic extractants di-2-ethylhexyl-phosphoric acid (D2EHPA) and mono-2-ethylhexyl phosphoric acid (MEHPA), with neutral extractants like tri-n-butyl phosphate (TBP), is ideal for extracting Li^+ from brines characterized by low concentrations of divalent ions (Mg^{2+} and Ca^{2+}), such as the Salar de Atacama and Lake Zabuye brines[3]. While this method demonstrates greater selectivity for Li^+ over other monovalent ions like Na^+ and K^+, most solvents also show a strong affinity for divalent cations, such as Mg^{2+}, Ca^{2+} and Sr^{2+}, which are generally more abundant than Li^+ in geothermal and oilfield brines. As a result, pre-treatment steps are often necessary to remove these divalent cations and concentrate Li^+ prior to extraction[43].

To enhance Li selectivity, researchers have investigated the use of mixed extractants and synergistic systems, where combinations of acidic and chelating extractants improve the separation efficiency by reducing the co-extraction of impurities[58,59]. A synergistic solvent extraction system comprising a liquid ion exchanger (saponified bis(2-ethylhexyl)dithiophosphoric acid) and a lithium-selective ligand (2,9-dibutyl-1,10-phenanthroline) in an aliphatic diluent has shown high selectivity for lithium ion over other alkali and alkaline earth ions[59]. This system has demonstrated impressive separation factors: 620 ± 20 for Li^+/Na^+, 3100 ± 200 for Li^+/K^+, 596 ± 9 for Li^+/Mg^{2+}, and 2290 ± 80 for Li^+/Ca^{2+} in a synthetic geothermal brine[59]. Similarly, a novel synergistic deep eutectic solvent (DES) concept has been proposed for improving the performance of environmentally benign liquid-liquid extraction of Li[58]. This approach combines two different conventional extractants, a beta-diketone and a neutral extractant, to create a synergistic DES with lower viscosity than conventional hydrophobic ionic liquids[58]. The extraction capacity of Li reached 4.4 $g{\cdot}L^{-1}$ using the optimum DES combination, also demonstrating highly selective recovery of lithium over sodium and potassium in a model brine solution[58].

Solvent extraction can achieve high Li recovery efficiencies, with Li recovery rates ranging from 80% to 99.9%[60]. Additionally, the method generates minimal solid waste compared to other extraction techniques, reducing its environmental footprint. The technology is also well-established in other industries, which may facilitate its adaptation for Li recovery. These attributes make solvent extraction an attractive option for Li extraction, particularly in brines with favorable chemistry. However, these advantages are counterbalanced by several significant challenges. The high cost of solvent replenishment (~$2800 per ton LCE)[61] is a primary economic barrier, particularly in brines with high impurities, like Ca and Mg, and low Li concentrations[3,43]. Additionally, organic solvent leaks pose environmental hazards, while the corrosive additives used in the process can damage equipment and generate large volumes of acid wastewater and potentially toxic organic waste[43,62]. Post-treatment steps are necessary to remove residual solvents before disposal, adding to the operational complexity[43]. The combination of these economic, environmental, and technical challenges currently limits the viability of solvent extraction for Li recovery from low Li-bearing brines.

Membranes. Membrane processes (Fig. 5b) particularly reverse osmosis (RO), nanofiltration (NF), and electrodialysis (ED), have been widely applied in water treatment and are increasingly explored for Li extraction[3,63]. These methods effectively separate substances based on their ionic radii; for example, membranes allow smaller ions to pass through while retaining larger ones, taking advantage of the selective permeability of the membrane materials[64]. The separation mechanism relies on pressure, concentration gradients, or electric potential differences to drive solutions through the membranes[65,66].

The challenge in Li extraction lies in the similar ionic radii of Mg^{2+} (0.072 nm) and Li^+ (0.069 nm)[67], necessitating the utilization of the Donnan exclusion effect for effective separation[64]. Positively charged membranes can reject positively charged ions, with the rejection rate increasing for ions with higher charges[68,69]. Therefore, controlling the pore size and using membranes with a positive surface charge are crucial for achieving effective Li^+/Mg^{2+} separation[64]. Recent advancements in membrane technology have focused on improving selectivity in the presence of impurities. For example, a bioinspired membrane in a low-grade brine demonstrated ultrahigh Li^+/Na^+, Li^+/K^+, Li^+/Mg^{2+}, and Li^+/Ca^{2+} selectivities of 737, 198, 1525116, and 3274, respectively[70].

One of the main advantages of membrane-based Li extraction is its ability to operate continuously, reducing downtime compared to batch processes[63]. Additionally, membrane systems offer scalability with a moderate cost (~$3000 per ton LCE)[71], allowing for flexible deployment across various brine compositions. Unlike chemical-based methods, membrane processes do not require chemical regeneration, making them more environmentally sustainable and operationally simpler. Despite these advantages, membrane-based Li extraction faces several significant challenges. Membrane fouling, caused by organic compounds and other brine impurities, reduces permeability and efficiency over time[48,62,63]. For instance, Somrani et al. observed a 50% reduction in membrane permeability after 6 hours of filtration due to fouling[72]. This membrane fouling (degradation) further impacts long-term performance, necessitating frequent maintenance and replacement. Additionally, the operational costs for membrane processes can be substantial, as generating the required pressure or electric gradients demands significant energy input. Even in brines with relatively high Li concentrations, Li recovery rates typically remain below 80%, and efficiency declines further in complex brines with high impurity levels[48]. These economic and technical barriers currently limit the widespread adoption of membrane-based Li extraction for direct Li recovery from brines.

Electrochemistry. Electrochemical methods (Fig. 5c) have emerged as an environmentally sustainable and energy-efficient strategy for Li extraction, inspired by the operational principles of lithium-ion batteries. These methods utilize redox-active materials, such as spinel-structured $LiMn_2O_4$ (LMO-type) and olivine-structured $LiFePO_4$ (LFP-type), as working electrodes to selectively capture and release Li^+ ions from solution under an applied electric field[62]. A typical electrochemical Li extraction system consists of Li-selective electrodes, ion-exchange membranes, and an electrolyte. By applying an external electric field, Li^+ is directed toward the electrode or through a Li-selective membrane, taking advantage of their distinct ionic radius, charge density, and electrochemical properties. The process generally involves three critical stages: (1) electrochemical adsorption (discharging), where Li^+ is selectively intercalated into electrode as shown in *reactions* 1*a*[73,74] *and* 1*b*[75]; (2) Li concentration, where Li^+ is accumulated in a designated compartment

Table 2 | Comparison of direct lithium extraction (DLE) technologies: solvent extraction, membrane, electrochemistry, adsorption, and ion exchange

Method	Cost (US $/ton LCE)	Mechanism	Maturity	Li Recovery Rates	Li Selectivity	Advantages	Challenges
Solvent Extraction	~2800	Li^+ is selectively extracted into an organic phase containing Li-selective extractants. Stripping regenerates the solvent.	Precommercial	80–99.9%	Low to moderate	Low solid waste production; Well-established in other industries.	Some solvents are infeasible in brines with high impurities (e.g., Mg and Ca), or diluted Li; Expensive relative to other technologies; High solvent cost and ongoing replenishment needed; Toxic organic waste disposal issues; Potential environmental hazards from solvent leaks; Post-treatment is required to remove residual solvent before disposal.
Membrane	~3,000	Li^+ is separated from other ions via size exclusion (nanofiltration, reverse osmosis) or electrostatic attraction (electrodialysis).	Precommercial	80%	Moderate	Continuous operation, reducing downtime; Scalable and modular, allowing flexible deployment; No chemical regeneration needed.	Membrane fouling from brine impurities; High energy consumption for pressure-driven systems; Limited Li recovery efficiency in complex brines.
Electrochemistry	~4,050	Li^+ intercalation/deintercalation at electrodes under applied voltage.	Precommercial	90%	Low to moderate	Low chemical consumption reduces reagent costs; Low water consumption and waste generation along with good control over the production rate; Environmentally friendly compared to solvent-based methods.	High energy demand for electrode operation; Low selectivity of Li; Electrode degradation over multiple cycles; High initial CAPEX for specialized equipment.
Adsorption	2800–3600	Li^+ is adsorbed onto the positively charged layers of LDHs, with anion exchange balancing charge.	In use commercially	80–99.9%	High	Commercialization achieved; High Li selectivity in brines with low Mg/Li; Lower chemical consumption compared to ion exchange; Environmentally friendly, does not produce secondary waste.	Li pre-concentration step may be required; Required temperatures >40 °C; Limited capacity per cycle, requiring frequent regeneration; Decreased performance in high-Mg brines; Slow kinetics compared to ion exchange.
Ion Exchange	3200–4600	Li^+ exchange with H^+ in ion exchangers. Acid washing regenerates the material.	Precommercial	75–99.9%	High	Fast Li uptake kinetics; Higher Li uptake per cycle; Superior Li selectivity and separation efficiency in brines with high Mg/Li; Lower energy and water consumption.	Pre-treatment of organic compounds removal is needed; Requires acid/base for regeneration, increasing operational cost; Material dissolution reduces adsorbent lifespan; Performance degrades over cycles due to structural changes.

Source: The Goldman Sachs Group, Inc[43]., McKinsey & Company[60], Warren[61], Kong et al.[80] and Farahbakhsh et al.[71].

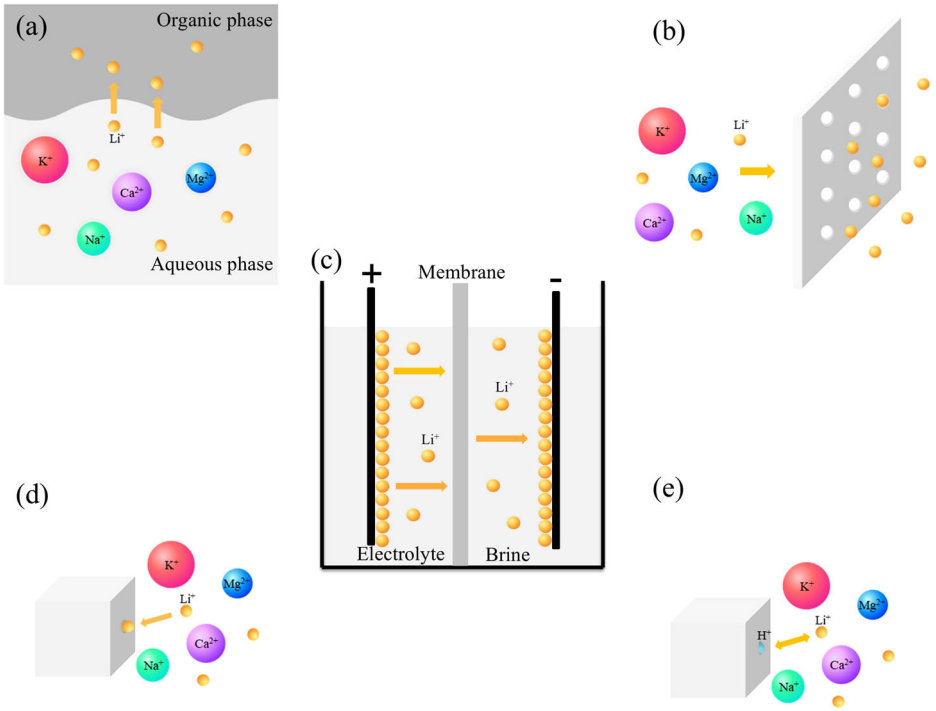

Fig. 5 | Lithium extraction mechanisms from aqueous solutions. Schematic illustrations of common DLE methods: **a** Solvent extraction; **b** membrane; **c** electrochemistry; **d** adsorption; **e** ion exchange.

or deposited on the electrode surface; and (3) electrochemical desorption (charging), where Li^+ is released into a recovery solution by reversing the applied potential or modifying the electrochemical conditions, as shown in *reactions 2a*[73,74] *and 2b*[75].

Discharging:

$$Li^+ + FePO_4 + e^- \rightarrow LiFePO_4 \quad (1a)$$

$$Li^+ + \lambda{-}Mn_2O_4 + e^- \rightarrow LiMn_2O_4 \quad (1b)$$

Charging:

$$LiFePO_4 \rightarrow Li^+ + FePO_4 + e^- \quad (2a)$$

$$LiMn_2O_4 \rightarrow Li^+ + \lambda{-}Mn_2O_4 + e^- \quad (2b)$$

Recent studies have explored the use of $LiFePO_4/FePO_4$ as electrodes for Li recovery from high-Mg brines, seawater, and geothermal water. Liu et al. utilized $LiFePO_4/FePO_4$ as electrode materials to extract Li from brines with high Mg/Li ratios, achieving a Li uptake capacity of 38.9 $mg{\cdot}g^{-1}$ under the optimal conditions[74]. These conditions included an initial Li concentration of 200 $mg{\cdot}L^{-1}$ in the anolyte, an anode–cathode distance of 2 cm, an electrolyte temperature 25 °C, a surface density of active substrate 18 $mg{\cdot}cm^{-2}$, and an electrolysis time of 900 minutes[74]. To further enhance Li selectivity and reduce intercalation overpotential, Liu et al. developed pulsed-rest and pulse-rest-reverse pulse-rest electrochemical intercalation techniques using TiO_2-coated $FePO_4$ electrodes for Li extraction from seawater[76]. Notably, the pulse-rest-reverse pulse-rest approach also improved the stability of the electrode's crystal structure during Li and Na co-intercalation[76]. Sun et al. modified $LiFePO_4/FePO_4$ with PEG-6000 to introduce a porous structure, enabling its application in Li recovery from low-concentration (25.78 $mg{\cdot}L^{-1}$ Li^+) geothermal waters[77]. The modified electrodes demonstrated a Li adsorption capacity of 17.10mg g^{-1} and a Li recovery rate reached 90.65% after eight adsorption-desorption cycles, while maintaining structural stability throughout the process[77]. $LiMn_2O_4/\lambda$-Mn_2O_4 has also been investigated for Li recovery. For example, Xu et al. utilized $LiMn_2O_4/\lambda$-Mn_2O_4 to recover Li from Da Qaidam brine, reporting a manganese dissolution rate of <0.077% per cycle and a retention of 91% of the initial intercalation capacity after 100 cycles, which is significantly lower than the 4.14% dissolution rate observed in the manganese-based ion exchange method[75].

LMO and LFP have been extensively compared for electrochemical Li extraction, each with distinct advantages and limitations[78]. LMO demonstrates high Li selectivity; however, its instability in acidic environments and susceptibility to water splitting side reactions impede its practical application unless modifications are made to improve its durability[78]. In contrast, LFP offers superior stability and resistance to degradation, making it a more reliable choice for large-scale Li extraction, particularly across varying pH conditions. While LMO may be preferable when Li selectivity is the primary concern, LFP remains the material of choice for long-term, stable operation.

Electrochemical methods present several environmental and economic benefits, such as low chemical consumption, reduced water usage, and minimal waste generation[63]. Moreover, they enable precise control over Li production rates, improving operational stability. However, a significant challenge is low Li selectivity. Zhao et al. investigated this issue with LFP and found that applying a lower voltage enhanced the separation of Mg and Li, although the Li uptake capacity of $LiFePO_4/FePO_4$ decreased as Mg concentration increased[73]. Similarly, Guo et al. observed that higher Mg concentrations led to a reduction in Li uptake capacity while simultaneously increasing the uptake of Mg when employing $LiMn_2O_4/Li_{1-x}Mn_2O_4$[79]. The order of the negative effects of cations is $Mg^{2+} > Na^+ > Ca^{2+} > K^+$[79]. The long-term viability of electrochemical Li extraction remains constrained by electrode degradation, high energy consumption, and the costs associated with electrode materials and system maintenance. Electrochemistry is the most expensive DLE method (~$4050 per ton LCE)[80]. Continued research into advanced electrode designs and optimized operating conditions holds significant potential to overcome these challenges.

In parallel, advancements in electrochemical methods, such as the low-temperature electrolysis process described in a recent patent[81], offer an alternative approach to producing high-purity Li metal without the need for high-temperature purification steps. This method uses a non-aqueous electrolyte composition, including phenyl trihaloalkyl sulfone and an organic cation bis(trihaloalkylsulfonyl)imide, making it suitable for DLE applications. Similarly, the work by Bernini et al. describes an electrochemical process for producing lithium-aluminum (LiAl) intermetallic from a LiCl ionic liquid melt at low temperatures[82]. LiAl can be easily

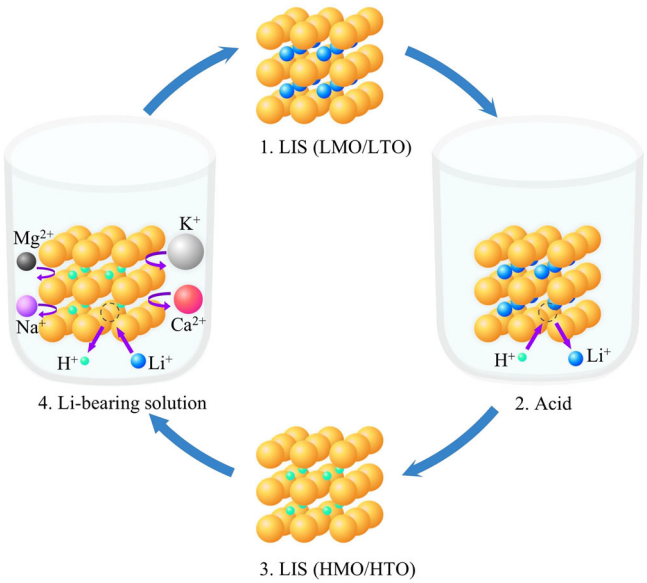

Fig. 6 | Schematic representation of the Li recovery process using LMO or LTO ion sieves and the ion sieve effect. The process involves acid treatment (delithiation, step 2) of LIS (LMO/LTO) to regenerate LIS (HMO/HTO), followed by Li recovery (lithiation, step 4) from Li-bearing solution using the generated LIS (HMO/HTO). The diagram also illustrates the regeneration of the LIS material (LMO/LTO) for subsequent cycles.

converted to Li_2CO_3 when it reacts with water and CO_2. These innovative approaches complement electrochemical Li extraction technologies, offering potential pathways for improving efficiency and purity in Li production and utilization.

Adsorption. Adsorption (Fig. 5d) is a process in which molecules of a substance adhere to the surface of a solid or liquid material due to physical forces or chemical bonds. It is typically reversible, with the opposite process known as desorption. Adsorption-based methods are widely used in applications that include water and air purification. In the context of DLE, aluminum hydroxide adsorbents, with the general chemical formula $[LiAl_2(OH)_6]Cl{\cdot}nH_2O$, referred to as lithium-aluminum-layered double hydroxide chloride (LiAl-LDH), are the most extensively studied materials for Li separation via adsorption[48]. LiAl-LDH is synthesized by inserting Li salts, such as LiCl, into gibbsite ($Al(OH)_3$). Its structure consists of positively-charged layers with Li^+ and Al^{3+} cations coordinated by OH^- anions, while Cl^- anions and water molecules occupy the interlayer spaces. During the adsorption process, Li^+ fills vacancies on the layered plates, serving as adsorption sites, while the accompanying Cl^- remains in the interlayer spaces to maintain charge balance[83]. The loaded adsorbent is then rinsed with a diluted LiCl solution to eliminate undesired ions, followed by a second rinse to recover the adsorbed Li^+.

Adsorption-based Li extraction is one of the most advanced and commercially implemented DLE technologies, with costs ranging from $2800 to $3600 per ton of Li_2CO_3[43,60,61]. This method offers high Li recovery rates (80–99.9%) and has been successfully deployed in commercial operations. It demonstrates strong Li selectivity in brines with low Mg/Li ratios, reducing chemical consumption and minimizing secondary waste generation. A recent study using LiAl-LDH revealed that 91% of Li was extracted from a geothermal brine solution, also demonstrating excellent Li^+ selectivity of 47.8 compared to Na^+ and 212 compared to K^+[84]. This selectivity occurs because the larger alkali ions are unable to fit into the octahedral sites of the LDH structure. These attributes make adsorption-based Li extraction a promising approach, particularly in regions where brines have favorable Mg/Li ratios and operating conditions. Despite its commercialization, adsorption-based DLE faces several limitations. A significant challenge with LiAl-LDH adsorbents is their tendency to degrade into unreactive gibbsite occurs when the charge balance of the interlayers is disrupted, typically caused by excessive removal of LiCl during delithiation. This degradation compromises the reusability of the adsorbents. To prevent this, maintaining the chemical stability (structure) of the adsorbents requires the use of a LiCl eluate during the regeneration process. Additionally, LiAl-LDH adsorbents have a limited Li adsorption capacity per cycle (<7 $mg{\cdot}g^{-1}$) and limited selectivity, necessitating frequent regeneration, and its performance declines in brines with high Mg/Li ratios[48]. The slower kinetics of adsorption compared to ion exchange may also impact overall throughput, posing challenges for high-demand Li recovery operations. For example, Jiang et al. studied the kinetics of Li adsorption on LiAl-LDH adsorbents; Li adsorption reached equilibrium in 10 hours at an adsorption capacity of 3.0 $mg{\cdot}g^{-1}$[85]. Consequently, the process also necessitates Li pre-concentration, which increases operational costs, and typically requires elevated temperatures (>40 °C) to improve kinetics[43]. Despite these drawbacks, LiAl-LDH remains the only material currently utilized in commercial-scale DLE applications[86–88].

Ion exchange. Ion exchange (Fig. 5e) sorbents are inorganic materials that contain template ions, which are incorporated into an inorganic compound through redox or ion exchange reactions[3]. Since they are synthesized in the presence of templated ions, only target ions with ionic radii and dehydration energies comparable to or smaller than those of the template ion can access the crystal sites. Ion exchange materials recover Li from aqueous solution through two mechanisms: physisorption, which is facilitated by weaker electrostatic forces and results in the general accumulation of Li near the surface of the sorbent, and chemical adsorption via ion exchange, which is strongly dependent on solution pH and often results in the intercalation of Li into solid state sorbents[3,89].

In DLE applications, ion exchange sorbents, also known as lithium ion-sieves (LISs), predominantly refer to hydrogen manganese oxides (HMOs) and hydrogen titanium oxides (HTOs). These materials are derived from LMOs and lithium titanium oxides (LTOs), respectively. Lithium recovery processes utilizing LMOs or LTOs follow a circular, pH-dependent ion exchange process, often referred to as the "LIS effect", as shown in Fig. 6. Before being used to recover Li from a Li-bearing solution, the LIS precursor is treated with an acidic solution to remove the Li^+ from the ion exchange sites and replace it with protons (H^+). Subsequently, the material is immersed in a Li-bearing solution adjusted to mildly alkaline conditions, where Li^+ is adsorbed onto the LIS. The LIS is highly selective toward Li^+ over other common coexisting major cations such as Mg^{2+}, Ca^{2+}, Na^+, and K^+ due to the small ionic radius of Li^+. Despite the similar ionic radii of Mg^{2+} (0.072 nm) and Li^+ (0.069 nm)[67], LIS materials are less selective toward Mg^{2+} because of its nearly four times higher hydration energy (−1922 kJ mol^{-1}) compared to Li^+ (−515 kJ mol^{-1}). This energy barrier to dehydration hinders Mg^{2+} entering the LIS, favouring Li^+ uptake[90]. Once the Li^+ has been adsorbed, the LIS is regenerated by an acid desorption reaction that releases the adsorbed Li^+ into a small volume of acid, concentrating the former while most impurities are removed in the process.

The ion exchange method for Li extraction is a precommercial technology with significant potential, characterized by a cost range of USD$3200 to 4600 per ton of LCE[61]. Ion exchange achieves Li recovery rates of 75–99.9%[43,60,61], depending on the brine composition and operational parameters. Key advantages of ion exchange include rapid Li^+ uptake kinetics, high Li^+ uptake capacity per cycle, and exceptional Li^+ selectivity and separation efficiency, particularly in brines with high Mg/Li ratios. Studies have shown that LMOs and LTOs exhibit high selectivity for Li^+[91–93]. The equilibrium distribution coefficients of metal ions reveal that Li^+ is strongly favored, followed by Ca^{2+}, Mg^{2+}, Na^+, and K^+ in decreasing order of selectivity[91]. Additionally, the process exhibits lower energy and water consumption compared to alternative extraction methods. However, several challenges hinder its widespread adoption. The requirement for pretreatment to remove organic compounds adds complexity to the process, while the use of acid and base for regeneration increases operational costs

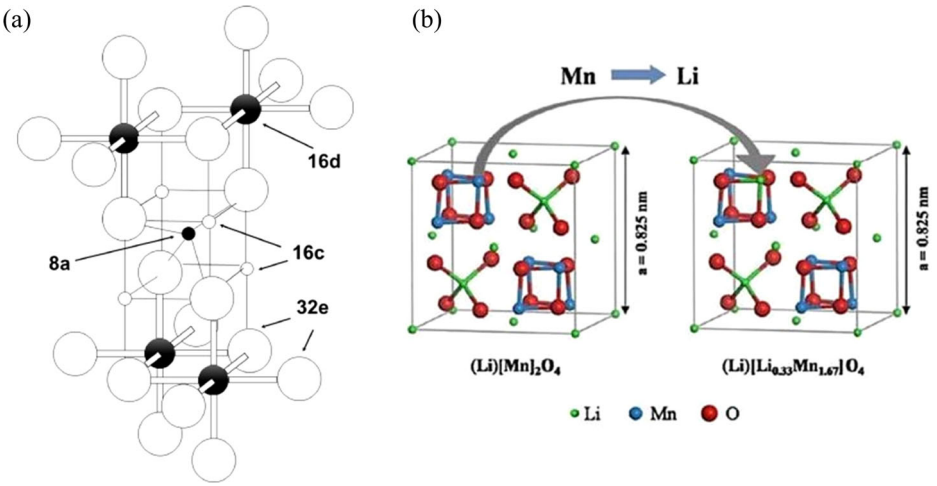

Fig. 7 | Crystal structure of spinel-type lithium manganese oxides. a Schematic representation of the spinel structure of $LiMn_2O_4$, illustrating the arrangement of Li in tetrahedral sites (8a), Mn in octahedral sites (16d), and oxygen ions in the cubic close-packed framework (32e). Adapted from Berg et al.[151]; **b** Modified spinel structure of $Li_{1.33}Mn_{1.67}O_4$, showing increased Li^+ occupancy in the 16c and 16d sites. Adapted from Murodjon et al.[152].

and introduces chemical handling concerns. Furthermore, material dissolution over time reduces the lifespan of the ion exchange material, and performance degradation due to structural changes during repeated cycles limits long-term efficiency. Despite these challenges, ion exchange remains a promising approach for Li extraction, particularly in applications where high selectivity and low energy consumption are critical.

Lithium manganese oxides

Spinel lithium manganese oxide has the general formula $LiMn_2O_4$, where Li occupies the tetrahedral sites (8a), and Mn occupies the octahedral sites (16d) in the cubic closed-packed oxygen framework (32e)[48] within the Fd-3m space group[94], as illustrated in Fig. 7a. In the ideal spinel structure of $LiMn_2O_4$, the 16c sites are octahedral interstitial sites that are typically vacant. However, these sites act as intermediate positions for Li^+ diffusion during lithiation/delithiation, as Li^+ diffuses through 8a→16c→8a→16c pathways (Fig. 7a) while preserving the overall structure of LMO[95]. The stoichiometric ratio of Li:Mn:O for a typical spinel LMO is 1:2:4. According to this ratio, the theoretical Li uptake capacity for $LiMn_2O_4$ is 40 $mg{\cdot}g^{-1}$. However, the stoichiometric ratio of Li:Mn can be modified to enhance the theoretical Li uptake capacity[3]. Generally, increasing the Li:Mn stoichiometric ratio in the precursor leads to an improvement in the theoretical Li uptake capacity. For example, $Li_{1.33}Mn_{1.67}O_4$ and $Li_{1.6}Mn_{1.6}O_4$ have theoretical Li uptake capacities of 60 $mg{\cdot}g^{-1}$ and 73 $mg{\cdot}g^{-1}$, respectively[48,94]. The increased theoretical Li uptake capacities of $Li_{1.33}Mn_{1.67}O_4$ and $Li_{1.6}Mn_{1.6}O_4$ are attributed to a decrease in trivalent manganese (Mn^{3+}) at the octahedral 16d sites by decreasing the overall disorder of the spinel through increases in Li^+ occupancy in 16c and 16d sites, as illustrated in Fig. 7b.

Recent studies have demonstrated that there are two Li sorption mechanisms for LMOs: a redox mechanism and an ion exchange mechanism, as expressed by *reactions* 3a and 3b, and 4, respectively[28]:

$$4(Li)\left[Mn^{3+}Mn^{4+}\right]O_4 + 8H^+ \rightarrow 3()\left[Mn_2^{4+}\right]O_4 + 4Li^+ + 2Mn^{2+} + 4H_2O \quad (3a)$$

$$()\left[Mn_2^{4+}\right]O_4 + nLiOH \rightarrow \left(Li_{n\,1-n}\right)\left[Mn_n^{3+}Mn_{2-n}^{4+}\right]O_4 + \frac{n}{2}H_2O + \frac{n}{2}O_2 \quad (3b)$$

$$Li_xMn_yO_4 + xH^+ \leftrightarrow H_xMn_yO_4 + xLi^+ \quad (4)$$

where () represents the tetrahedral sites (8a) and [] represents the octahedral sites (16d). Manganese in the LMO exists in both trivalent (Mn^{3+}) and tetravalent (Mn^{4+}) forms. Common LMOs include $LiMn_2O_4$, which contains an equal number of Mn^{3+} and Mn^{4+}, and $Li_{1.33}Mn_{1.67}O_4$ and $Li_{1.6}Mn_{1.6}O_4$, which contain exclusively Mn^{4+}. In general, Mn^{3+} in LMO represents the redox site, undergoing redox reactions during lithiation-delithiation cycles as indicated in *reactions* 3*a* and 3*b*. In contrast, Mn^{4+} represents the ion exchange site in LMO, as indicated in *reaction* 4. For an LMO containing both Mn^{3+} and Mn^{4+}, simultaneous redox and ion exchange processes take place.

Due to the specific electronic configuration of 3d orbitals, Mn^{3+} ($t_{2g}^3e_g^1$) is less symmetric than Mn^{4+} (t_{2g}^3) within the octahedral MnO_6 structure, primarily due to the Jahn-Teller effect[95]. Due to the 3d electronic configuration of Mn^{3+}, and in an octahedral crystal field, its degenerate e_g orbitals create an electronically unstable state[96,97]. To stabilize the system, the crystal lattice undergoes a distortion, typically elongating or compressing along one axis, which splits the degenerate orbitals into non-degenerate levels and lowers the overall energy. The most direct consequence of the Jahn-Teller effect is the elongation of the Mn–O bond along the z-axis within the MnO_6 octahedron (Fig. 8)[96], leading to a distortion of the crystal structure[97], also known as the Jahn-Teller distortion. LMO that contains Mn^{3+} tends to undergo such structural distortion. In addition to this, divalent manganese (Mn^{2+}) dissolution (loss) occurs when LMO is exposed to the desorption acids during delithiation (step 2 in Fig. 6, Fig. 9, *reaction* 3a) due to Mn^{3+} disproportionation into Mn^{2+} and Mn^{4+}. As a result, both Jahn-Teller distortion and Mn^{3+} disproportionation cause irreversible structural damage to LMO during lithiation-delithiation cycles[98], reducing its recyclability and shortening the sorbent lifespan. Therefore, LMOs with redox sites are not ideal for DLE applications. For economic feasibility in commercial Li production from low Li-bearing solutions, the sorbent must be reusable over multiple cycles. Additionally, LMOs with only ion exchange sites, such as $Li_{1.33}Mn_{1.67}O_4$ (60 $mg{\cdot}g^{-1}$) and for $Li_{1.6}Mn_{1.6}O_4$) (73 $mg{\cdot}g^{-1}$), have higher theoretical Li uptake capacities compared to redox-active LMOs like $LiMn_2O_4$ (40 $mg{\cdot}g^{-1}$)[94]. For these reasons, $Li_{1.33}Mn_{1.67}O_4$ and $Li_{1.6}Mn_{1.6}O_4$, comprised solely of Mn^{4+}, are gaining interest for advancing DLE applications.

In practical applications Li uptake often falls below theoretical values. This is due to its dependence on both the brine's chemistry and the properties of the LMO. Brines frequently contain impurities, such as other cations (e.g., Na^+, K^+, Mg^{2+}, Ca^{2+}) and organic compounds, that may interact with LMO, resulting in competition for Li^+ sorption sites. These competing interactions can reduce the efficiency of LMO in selectively extracting Li^+. Xiao et al. revealed that the presence of other metal cations decreased the Li uptake capacity of the LMO, with Na^+ and K^+ exhibiting less competitive sorption effects compared to Mg^{2+} due to the reasons discussed above[99]. Moreover, the physical properties of LMO, such as particle size, morphology, structural impurities and defects, can also impact Li^+ uptake. Larger LMO particles have smaller specific surface areas, limiting the material's interaction with Li^+ cations and consequently reducing its uptake capacity[100]. Furthermore, agglomeration or clustering of particles, which can occur during LMO synthesis or use, leads to pore plugging, diminishing the

accessible surface area and hindering Li uptake performance[101,102]. Similarly, the morphology of LMO, including nanorods, nanowires, cubic shapes, and spheres, which result from adjusting synthesis conditions, also affects the surface area and Li^+ uptake efficiency[95]. The presence of impurities and defects within the LMO structure can block Li^+ uptake sites or alter the minerals properties of the material, leading to reduced Li uptake capacities. For example, Wang et al. identified Mn_2O_3 impurities in LMO as the primary reason for decreasing Li uptake capacity[103].

Several studies utilizing LMO for lithium recovery are summarized in Table 3. Chitrakar et al. synthesized a $Li_{1.6}Mn_{1.6}O_4$ sorbent with a maximum Li uptake capacity of 40 mg·g^{-1} from seawater, despite the low Li concentrations (0.17 mg·L^{-1})[104]. Similarly, Shi et al. prepared a $Li_{1.6}Mn_{1.6}O_4$ sorbent that exhibited a maximum Li uptake capacity of 27.15 mg·g^{-1} at 50 °C[105]. Notably, Li uptake increased dramatically when the brine had a starting pH greater than 11, with both cases showing a comparable Mn loss of 2.5%. A spinel-type MnO_2 nanorod (Fig. 10a) with size ranging from approximately 40–90 nm in diameter and 150–900 nm in length was synthesized by Zandebakili et al. via a hydrothermal method[106]. This nanorod achieved a Li uptake capacity of 63 mg·g^{-1}, representing the highest value among all the LMO sorbents studied to date. In another study, Chitrakar et al. synthesized both $Li_{1.6}Mn_{1.6}O_4$ and $Li_{1.33}Mn_{1.67}O_4$ sorbents[107], which exhibited extremely high affinity for Li^+ in $NaHCO_3$-enriched brine (25 g $NaHCO_3$ in 1.0 L brine), with a Li uptake capacity of 27 mg·g^{-1} and Mn loss of only 0.5%. Seip et al. recovered Li from an oilfield brine using a $Li_{1.33}Mn_{1.67}O_4$ (Fig. 10b)[28]. Under optimized conditions (pH = 8, T = 70 °C), the sorbent achieved a Li uptake capacity of 18 mg·g^{-1}, with > 80% Li recovery within 30 minutes. However, Mn loss of 4.5% was relatively high due to the presence of Mn-reducing organic molecules in the brine and Mn reduction (Mn^{3+} formation) mainly happened on the particle surface, as evidenced from Fig. 10c. These studies highlight that LMOs can efficiently extract Li from brines, although the recurring issue of Mn reduction and dissolution during LMO cycling remains a concern.

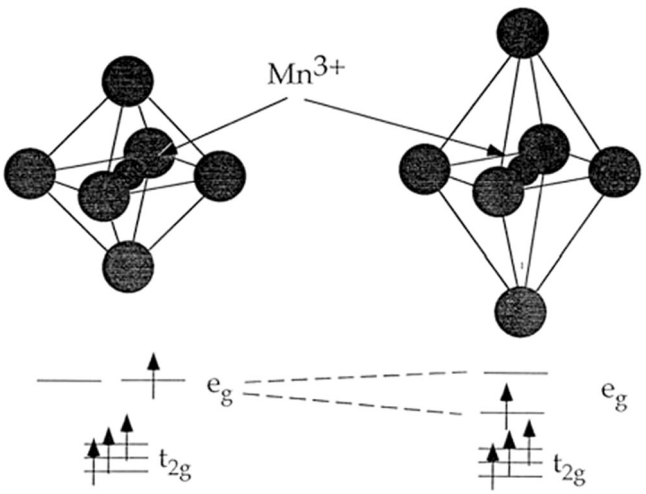

Fig. 8 | The Jahn–Teller distortion of an MnO_6 octahedron around Mn^{3+}. Adapted from Ceder et al.[96].

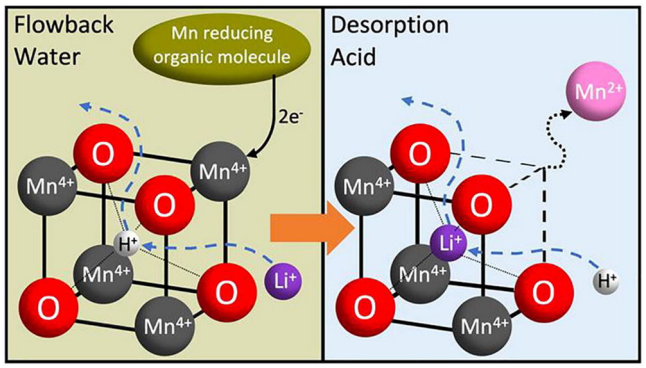

Fig. 9 | Schematic diagram of Mn^{4+} reduction in brines during lithiation and Mn^{2+} dissolution in acid during delithiation. Adapted from Seip et al.[28].

Modifications of LMO

Doping. Doping is a widely employed strategy to enhance the structural and electrochemical stability of LMO by incorporating specific elements into the spinel structure. This approach primarily aims to inhibit Mn reduction and stabilize Mn cations, thereby preventing their dissolution. Ideally, dopants replace Mn^{3+} in the 16d sites (Fig. 7a) of the spinel structure, establishing stronger bonds with oxygen[108], modifying the electron configuration of MnO_6 octahedra to mitigate Jahn-Teller distortion[97], or reducing the formation of electrochemically active Mn^{3+} and suppressing its disproportionation ($2Mn^{3+} \rightarrow Mn^{2+} + Mn^{4+}$)[109], a key process driving Mn^{2+} dissolution. Dopants such as Al^{3+}, Mg^{2+} and Ti^{4+} are particularly effective in mitigating Mn loss by strengthening the LMO lattice through the formation of stronger metal-oxygen bonds (e.g., Al-O, Mg-O or Ti-O bonds) compared to Mn-O bonds, reducing Mn migration and structural degradation[108,110]. In another study, europium (Eu^{3+}) has been shown to effectively suppress the Jahn-Teller effect through electron-orbital coupling, as shown in Fig. 11[97].

In LMO, partial substitution of Mn dopant ions could increase Li uptake capacity. While doping does not alter the fundamental spinel structure of LMO, it can modify lattice parameters. For instance, Ti^{4+} doping increases the lattice parameter due to the larger ionic radius of Ti^{4+} (0.061 nm) compared to Mn^{4+} (0.053 nm)[110]. This expansion of the unit cell facilitates Li^+ migration by reducing the migration resistance, as the larger cell size promotes easier tilting of the metal-O_6 octahedrons[111,112]. Moreover, the formation of stronger metal-O bonds weakens the Li-O bonds, further enhancing Li^+ mobility[113]. For example, Ti-O bonds (662 kJ mol^{-1}) are stronger than Mn-O (402 kJ mol^{-1}) bonds[114], and the weaker Li-O bond is favorable to Li^+ migration. These combined effects lead to a higher Li^+ diffusion coefficient and promote Li^+ transport, enhancing Li uptake capacity of the LMO. However, excessive dopant incorporation may lead to occupation of 8a sites[109], potentially reducing Li uptake capacity.

In DLE applications, previous studies have explored doping LMO with various cations (Table 4) via wet chemical or solid-state methods, including the use of monovalent cations (Na^+[115] and K^+[116]), divalent cations (Mg^{2+}[117] and Co^{2+}[118]), trivalent cations (Al^{3+}[119], Cr^{3+}[120], Fe^{3+}[121], and Ga^{3+}[122]), as well as tetravalent cations (Si^{4+}[123] and Ti^{4+}[124]). Qian et al. prepared LMOs doped with monovalent cations (Na^+ and K^+)[115,116]. Although these materials

Table 3 | Summary of the performance of LMOs

LMO precursor	Brine	pH	Li uptake (mg·g^{-1})	Mn loss (%)	Desorption acid	Reference
$Li_{1.6}Mn_{1.6}O_4$	Seawater, 0.17 mg·L^{-1}	-	40	2.5	0.5M HCl	104
$Li_{1.33}Mn_{1.67}O_4$	Urmia Lake, 12.7 mg·L^{-1}	11	63	1.01	0.5M HCl	106
$Li_{1.33}Mn_{1.67}O_4$/$Li_{1.6}Mn_{1.6}O_4$	$NaHCO_3$ added brine, 1600 mg·L^{-1}	6.6	27	0.5	0.5M HCl	107
$Li_{1.33}Mn_{1.67}O_4$	Oilfield brine, 43 mg·L^{-1}	8	18	4.5	0.5M H_2SO_4	28
$Li_{1.6}Mn_{1.6}O_4$	Salt lake brine, 266 mg·L^{-1}	5.35	27.15	2.5	0.5M HCl	105

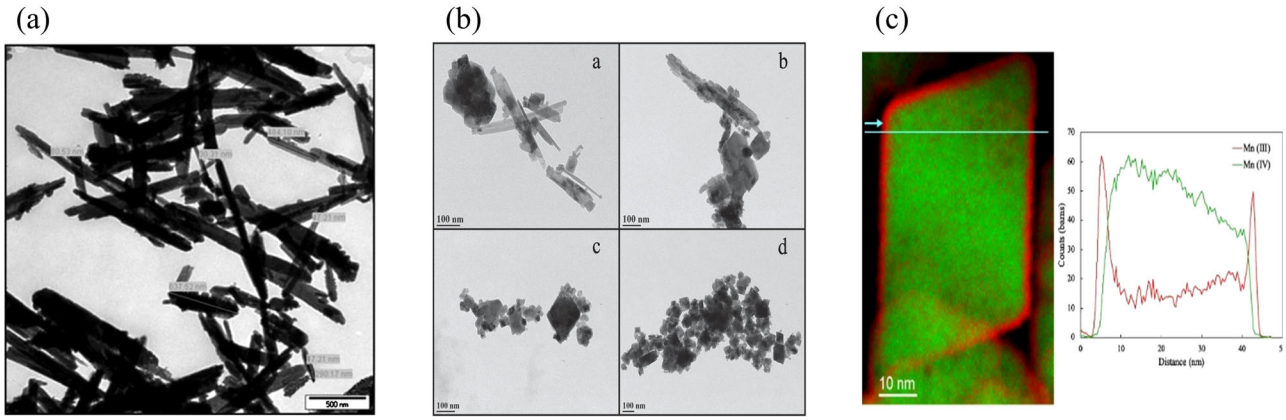

Fig. 10 | Morphology and elemental mapping of manganese-based lithium adsorbents. TEM images of **a** MnO_2 nanorod. Adapted from Zandevakili et al.[106]; **b** $Li_{1.33}Mn_{1.67}O_4$ with different particle shapes; **c** EELS mapping of $Li_{1.33}Mn_{1.67}O_4$ after lithiation in oilfield brine. Adapted from Seip et al.[28].

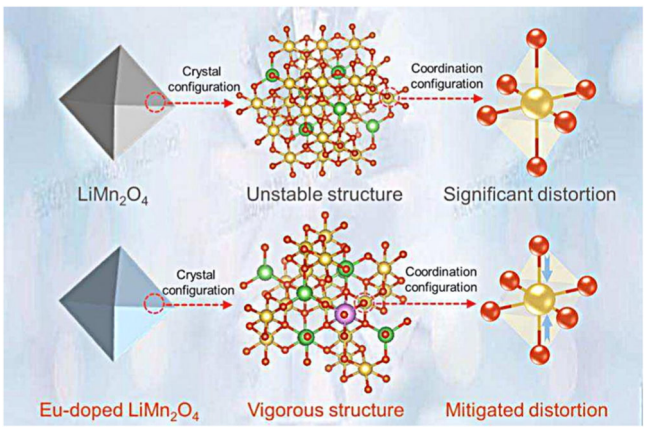

Fig. 11 | Schematic diagrams illustrating the structural evolution of $LiMn_2O_4$ and Eu-doped $LiMn_2O_4$ highlight the suppression of Jahn-Teller effect through Eu^{3+} incorporation[97].

demonstrated very similar Li uptake capacities to undoped LMO, both Na-doped LMO (4.4%) and K-doped LMO (4.0%) exhibited lower Mn loss compared to the undoped LMO (5.4%). It was found that Na^+ and K^+ primarily replaced Li^+ at the 16d sites, with Na^+ being more prone to replace surface Li^+ due to a lower formation energy, whereas K^+ favored bulk replacement. Additionally, Na-doped LMO and K-doped LMO retained 87.1% and 90.8% of their initial Li uptake capacities after six cycles, respectively. In the case of divalent cations such as Mg^{2+} and cobalt (Co^{2+}), both Mg-doped LMO and Co-doped LMO showed enhanced Li^+ adsorption performances[117,118]. Specifically, the Li uptake capacity of Mg-doped LMO increased from 33.2 $mg{\cdot}g^{-1}$ to 35.6 $mg{\cdot}g^{-1}$, and that of Co-doped LMO increased from 32.3 $mg{\cdot}g^{-1}$ to 35.4 $mg{\cdot}g^{-1}$. Conversely, Mn loss from Mg-doped LMO and Co-doped LMO decreased from 3.68% to 3.23% and from 5.43% to 4.42%, respectively. LMOs doped with trivalent cations also exhibited enhancements in both Li sorption and Mn stability. Zhang et al. reported a significant increase in Li uptake for Al-doped LMO, from 27.6 $mg{\cdot}g^{-1}$ to 32.6 $mg{\cdot}g^{-1}$, with a lower Mn loss (1.92%) compared to undoped LMO (2.06%)[119]. Similarly, chromium (Cr)-doped LMOs (Fig. 12) prepared by Cao et al. showed a significant enhancement in Li uptake capacity from 24.97 $mg{\cdot}g^{-1}$ to 31.67 $mg{\cdot}g^{-1}$ in a salt lake brine, retaining 81.7% of their initial Li uptake capacity after twenty cycles[120]. Chitrakar et al. synthesized Fe-doped LMOs through solid-state reactions, achieving 28 $mg{\cdot}g^{-1}$ of Li uptake in Salar de Uyuni brine with 1.1% Mn loss[121]. Furthermore, they maintained 90% of their initial Li uptake capacity after four cycles. Gallium (Ga)-doped LMOs, synthesized by Ju et al., showed a Li uptake capacity of 25.3 $mg{\cdot}g^{-1}$[122]. In the case of tetravalent cation doping, Ryu et al. synthesized titanium (Ti)-doped LMO and silicon (Si)-doped LMOs through solid-state methods[123,124]. The Si-doped LMO exhibited a superior Li uptake capacity of 43.23 $mg{\cdot}g^{-1}$, while the Ti-doped LMO showed an improved Li uptake capacity of 21.9 $mg{\cdot}g^{-1}$ compared to 19.6 $mg{\cdot}g^{-1}$ in the undoped LMO. These results suggest that doping can effectively enhance Li uptake and improve structural stability, addressing the challenges of Mn loss and advancing the commercial viability of LMOs.

Although doping is effective in reducing Mn loss, it remains relatively high (>1.1%) even after lithiation in organic-free solutions (Table 4). The substantial Mn loss observed in desorption solutions can be attributed to the use of HCl as the desorption fluid in the aforementioned studies[125]. Herrmann et al. compared Mn loss in various desorption fluids after lithiation from a geothermal brine, including ammonium peroxydisulfate ($(NH_4)_2S_2O_8$), sodium peroxydisulfate ($Na_2S_2O_8$), acetic acid (CH_3COOH), carbonic acid (H_2CO_3), ascorbic ($C_6H_8O_6$), H_2SO_4 and HCl[125]. The results indicated that the Mn loss followed the order: $C_6H_8O_6$> HCl> H_2SO_4> $Na_2S_2O_8$> CH_3COOH> H_2CO_3> $(NH_4)_2S_2O_8$, with HCl and H_2SO_4 demonstrated over 95% Li stripping efficiency[125]. Additionally, using HCl as the desorption fluid results in alkali metal ions forming their chloride salts, which minimizes the precipitation salts other than Li_2CO_3 during the separation of Li[126]. For these reasons, researchers often use HCl as the desorption fluid.

Surface coating. Compared to doping methods, surface coating represents a more recent approach to optimizing DLE materials. Surface coating involves applying a protective layer to the material's surface to shield it from the surrounding environment. In DLE applications, this coating acts as a physical barrier, preventing direct contact between the LMO and Mn-reducing agents such as organic compounds and H_2S commonly found in brines. Selecting a coating layer with an optimal porosity allows for the diffusion of small Li^+ cations while blocking larger organic molecules that could otherwise come into contact with the LMO and reduce Mn^{4+} to Mn^{3+}. The choice of coating material is critical, as it must ensure chemical stability in both the brine and desorption acid, providing effective long-term protection against Mn loss.

Inorganic coatings, often referred to as metal oxide coatings, are particularly effective for allowing Li^+ to diffuse without significant resistance due to their short diffusion paths, amorphous defects, crystalline channels, optimal thickness, and enhanced interfacial conductivity. This concept has been extensively studied in the context of surface modification for cathode materials in battery applications[127–130]. Such coatings, typically a few nanometers thick, provide short diffusion paths for Li^+. The diffusivity of Li^+ remains unchanged up to an optimal thickness, beyond which it decreases due to increased resistance[128]. While the amorphous nature of these layers often introduces defects such as vacancies, micropores, and grain boundaries, which act as low-energy pathways for ion migration[129], some

Table 4 | Performances of LMOs doped with various elements

Dopant	LMO precursors	Brine	pH	Li uptake (mg·g^{-1})	Mn loss (%)	Desorption acid	Recyclability	Reference
Na^{+}	$Li_{1.6}Mn_{1.6}O_4$	LiCl solution, 168 (mg·L^{-1})	12	33.9	4.4	0.6 M HCl	6 cycles, 87.1%	115
K^{+}	$Li_{1.6}Mn_{1.6}O_4$	LiCl solution, 42 (mg·L^{-1})	12	26.0	4.0	0.6 M HCl	6 cycles, 90.8%	116
Mg^{2+}	$Li_{1.6}Mn_{1.6}O_4$	Salt lake brine, 156 (mg·L^{-1})	-	35.6	3.2	0.5M HCl	10 cycles, 65.7%	117
Co^{2+}	$Li_{1.6}Mn_{1.6}O_4$	LiCl solution, 84 (mg·L^{-1})	12	35.4	4.4	0.3M HCl	5 cycles, 82.9%	118
Al^{3+}	$Li_{1.6}Mn_{1.6}O_4$	LiOH solution, 350 (mg·L^{-1})	-	32.6	1.9	0.5M HCl	4 cycles, 82.2%	119
Cr^{3+}	$Li_{1.6}Mn_{1.6}O_4$	Salt lake brine, 222.2 (mg·L^{-1})	-	31.7	2.1	0.5M HCl	20 cycles, 81.7%	120
Fe^{3+}	$Li_{1.33}Mn_{1.67}O_4$	Salar de Uyuni, 1630 (mg·L^{-1})	8.2	28.0	1.1	0.5M HCl	4 cycles, 90%	121
Ga^{3+}	$LiMn_2O_4$	LiCl solution, 50 (mg·L^{-1})	9	25.3	4.7	0.1M HCl	8 cycles, 68.25%	122
Si^{4+}	$Li_{1.33}Mn_{1.67}O_4$	Li spiked seawater, 60 (mg·L^{-1})	-	43.2	1.5	0.3M HCl	-	123
Ti^{4+}	$Li_{1.33}Mn_{1.67}O_4$	Li spiked seawater, 60 (mg·L^{-1})	-	21.9	3.3	0.3M HCl	5 cycles, 88.7%	124

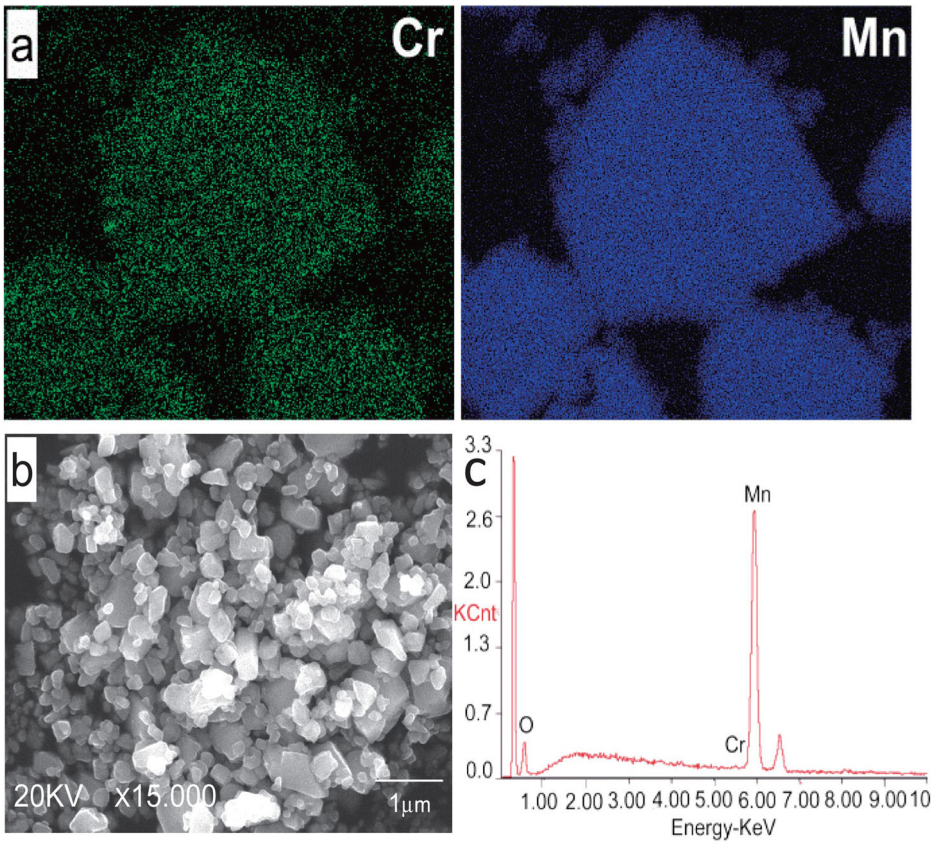

Fig. 12 | Characterization of Cr-doped LMO. **a** EDS mapping of Cr and Mn from $Li_{1.6}Mn_{1.6-x}Cr_xO_4$ (x = 0.016); **b** SEM of $Li_{1.6}Mn_{1.6-x}Cr_xO_4$; **c** EDS result of $Li_{1.6}Mn_{1.6-x}Cr_xO_4$. Adapted from Cao et al.[120].

crystalline coatings, like θ-Al_2O_3, have highly diffusive one-dimensional channels that allow for low Li^+ migration barriers[130]. Lu et al. demonstrated that amorphous Al_2O_3, ZrO_2, and ZnO coatings exhibit low Li^+ diffusion barriers in a Li-ion battery[129]. Additionally, the authors highlighted a trend in Li^+ diffusion barriers for crystalline coatings based on their space groups: metal oxides within $la\bar{3}$ space group exhibit relatively low Li^+ diffusion barriers compared to those in the $Fm3m$ and $R\bar{3}c$ space groups[129]. Surface diffusion along the coating and enhanced conductivity at the interface between the coating and the active material facilitate smooth Li^+ transport. For example, ZrO_2 is an excellent conductor of Li^+ and H^+, which facilitates the ion exchange reaction of Li^+ and H^+[131]. Overall, the combination of amorphous structure, optimal thickness, and interfacial properties ensures that Li^+ ions can diffuse through the inorganic layer with minimal resistance, while providing excellent protection to LMO.

Building on these advantages, inorganic oxide compounds such as SiO_2, ZrO_2, Al-oxide, and Ni-oxide (Table 5) have emerged as common coating materials for improving the performance of LMO in DLE applications. For example, Wang et al. synthesized a ZrO_2-coated LMO for extracting Li from the Qinghai Kunty salt lake brine, which has a high Mg/Li mass ratio of 65-70. Their results demonstrated that the ZrO_2-coated LMO had lower Mn loss (0.349%) and a higher Li uptake capacity (25.96 mg·g^{-1}) compared to the bare LMO, which had a Mn loss 0.89% and a Li uptake capacity of 28.88 mg·g^{-1}[131]. Ohashi and Tai found that applying a 10–20 nm coating of Al-oxide or Ni-oxide on LMO reduced Mn loss by 10-30% during both the protonation and delithiation processes[132]. However, the advantages of this protective layer tended to diminish in subsequent extraction cycles. Li et al. optimized an LMO coated with 25 nm of SiO_2 (Fig. 13) and calcined at 500 °C, achieving a Li uptake capacity of 18.5 mg·g^{-1}, while decreasing Mn loss by 45–50% compared to bare LMO[133]. Even after seven cycles, this coated LMO retained a Li uptake capacity of 15.3 mg·g^{-1}.

Attaining a uniform coating thickness and coverage across the entire surface of the LMO is challenging but crucial for maintaining

Table 5 | Performances of LMOs coated with various materials

Coating material	LMO precursors	Brine	pH	Li uptake ($mg \cdot g^{-1}$)	Mn loss (%)	Desorption acid	Recyclability	Reference
SiO_2	$LiMn_2O_4$	Salt lake brine, 384 ($mg \cdot L^{-1}$)	9	18.5	6.3	0.1 M HCl	7 cycles, 82.7%	133
ZrO_2	$Li_{1.6}Mn_{1.6}O_4$	Salt lake brine, 65-70 ($mg \cdot L^{-1}$)	-	25.96	0.349	0.1 M HCl	15 cycles, 92.2%	131
Al-oxide	$Li_{1.33}Mn_{1.67}O_4$	Natural brine, 1470 ($mg \cdot L^{-1}$)	6.5	42.5	0.8	0.25M H_2SO_4	4 cycles, ~85%	132
Ni-oxide	$Li_{1.33}Mn_{1.67}O_4$	Natural brine, 1470 ($mg \cdot L^{-1}$)	6.5	45	0.9	0.25M H_2SO_4	4 cycles, ~80%	132

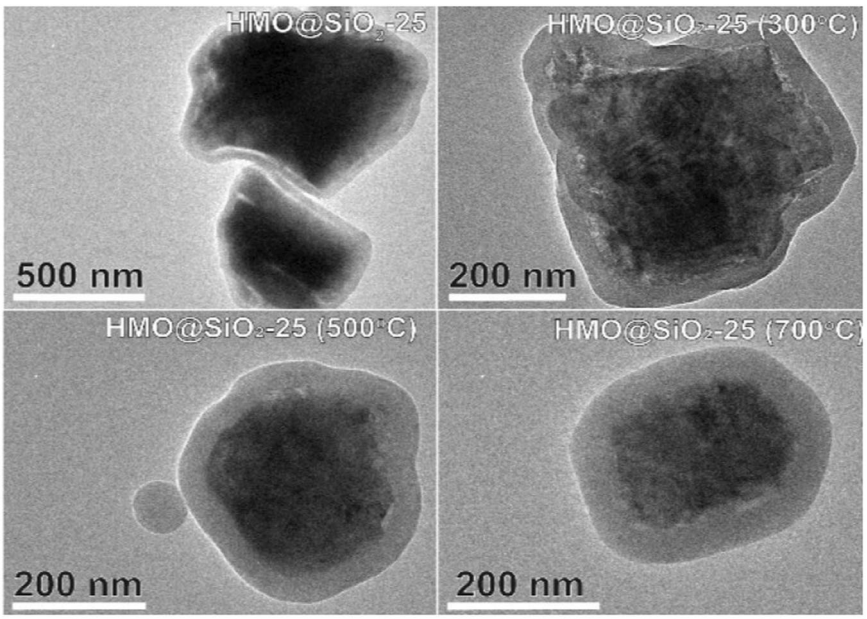

Fig. 13 | TEM images of LMO coated with 25 nm of SiO_2. Reprinted (adapted) with permission from Li et al.[133].

consistent performance and optimizing Li extraction efficiency[134–136]. Non-uniform coatings can cause reduced Li recovery efficiency and greater Mn dissolution. Furthermore, the cost-effectiveness of surface coating methods needs careful consideration[135,136], particularly for large-scale DLE applications. Both coating materials and techniques should be economically viable, ensuring that they do not significantly increase the overall cost of Li extraction[135,136]. Scalability is another important issue, as coating deposition techniques, equipment, and material properties[137,138], potentially complicating the transition from lab-scale to industrial production. Recycling degraded LMO with coating presents additional challenges. While a bare LMO can be easily dissolved in hydrometallurgical recycling processes[139–141], allowing its constituent elements to be recovered and reused, coated LMOs are more resistant to dissolution. This resistance necessitates extra steps to separate the coating materials from the LMO elements during recycling, adding further complexity to the process.

LMO composites

The small size of LMO particles, typically within the nano-scale range, can lead to material loss during the recovery process, hindering their suitability for industrial applications. To address this issue, researchers have developed LMO composite materials. They can be synthesized by incorporating LMO nanoparticles in binding materials (Table 6), such as polyvinyl chloride (PVC)[142], polyacrylamide (PAM)[143], polyacrylonitrile (PAN)[144], polyvinyl alcohol (PVA)[145], polyvinylidene fluoride (PVDF)[146], alpha-alumina beads (AAB)[147], chitosan[148], and cellulose[149] through various synthesis methods, including granulation, foaming, magnetization, and membranization[150]. These approaches aim to improve the structural integrity and recovery efficiency of LMO particles, making them more suitable for large-scale, practical applications in DLE. It is important to note that the primary purpose of using composite materials is to immobilize and retain LMO nanoparticles on a substrate rather than mitigating Mn loss. Therefore, Mn loss is typically not documented in most of these studies and is not included in Table 6.

Zhu et al. developed a series of PVC-LMO membranes (Fig. 14a) using a solvent exchange method by adding LMO nanoparticles into a mixture of PVC and N,N-dimethyl acetamide (DMAc)[142]. The optimal membrane, containing 10 wt% PVC and 15 wt% LMO in DMAc, and with a liquid film thickness of 0.30 mm, was highly effective for Li recovery from aqueous solutions. Although embedding the LMO into the PVC-LMO membrane resulted in a 14% reduction in Li uptake capacity, it retained 98% of its initial capacity after eight cycles of use. Xiao et al. synthesized a granulated PAM-MnO_2 (Fig. 14b) through the inverse suspension polymerization method, using LMO, N,N-methylenebisacrylamide (MBA), and ammonium persulfate (APS) as the precursor, the solvent, and the initiator, respectively[143]. At 30 °C, the maximum Li equilibrium adsorption capacity reached 18.76 $mg \cdot g^{-1}$ in a synthetic LiCl brine. In the subsequent recycling test in the Qarhan brine, the PAM-MnO_2 film showed a lower Li uptake capacity of 4.34 $mg \cdot g^{-1}$, albeit with a slight decrease after 30 cycles, primarily attributed to film damage. Park et al. used PAN as a binder in a composite nanofiber-type PAN-LMO (Fig. 14c), produced via electrospinning[144]. The highest adsorption capacity achieved was 10.3 $mg \cdot g^{-1}$ with 60 wt% PAN-LMO, which exhibited less than 4% capacity loss over ten cycles, demonstrating excellent stability. Nisola et al. created a macro-porous, flexible PVA-LMO foam (Fig. 14d) through surfactant blending and cryo-desiccation, achieving Li uptake with minimal capacity loss (7-13%) when compared to LMO powder[145]. The best-performing PVA-LMO, loaded at 250 wt%, showed no loss in capacity after five adsorption-desorption cycles. Sun et al. fabricated a PVDF-LMO composite (Fig. 14e) with a high Li uptake capacity of 27.8 $mg \cdot g^{-1}$ within 1 hour, and a strong selectivity for Li^+ with a separation

Table 6 | Performances of LMO composites

Binder	LMO precursors	Brine	pH	Sorption time (hour)	Li uptake (mg·g^{-1})	Recyclability	Reference
PVC	$Li_{1.6}Mn_{1.6}O_4$	Artificial seawater, 150 (mg·L^{-1})	12	2	26.64	8 cycles, 98%	142
PAM	$Li_{1.33}Mn_{1.67}O_4$	Qarhan brine, 113 (mg·L^{-1})	6.4	20	4.34	30 cycles, slightly decrease	143
PAN	$Li_{1.6}Mn_{1.6}O_4$	LiCl/LiOH solution, 35 (mg·L^{-1})	11	24	10.3	10 cycles, 96.2%	144
PVA	$Li_{1.6}Mn_{1.6}O_4$	LiCl/LiOH solution, 7-35 (mg·L^{-1})	11	24	6.9	5 cycles, remain constant	145
PVDF	$Li_{1.33}Mn_{1.67}O_4$	LiCl solution, 100 (mg·L^{-1})	9	1	27.8	6 cycles, 91%	146
AAB	HMO	Li spiked seawater, 30 (mg·L^{-1})	7.8	72	21.7	14 cycles, 98%	147
Chitosan	$Li_{1.33}Mn_{1.67}O_4$	Li spiked seawater, 30.2 (mg·L^{-1})	7-8	72	11.4	-	148
Cellulose	HMO	LiCl solution, 75 (mg·L^{-1})	8.76	48	21.6	8 cycles, 83%	149

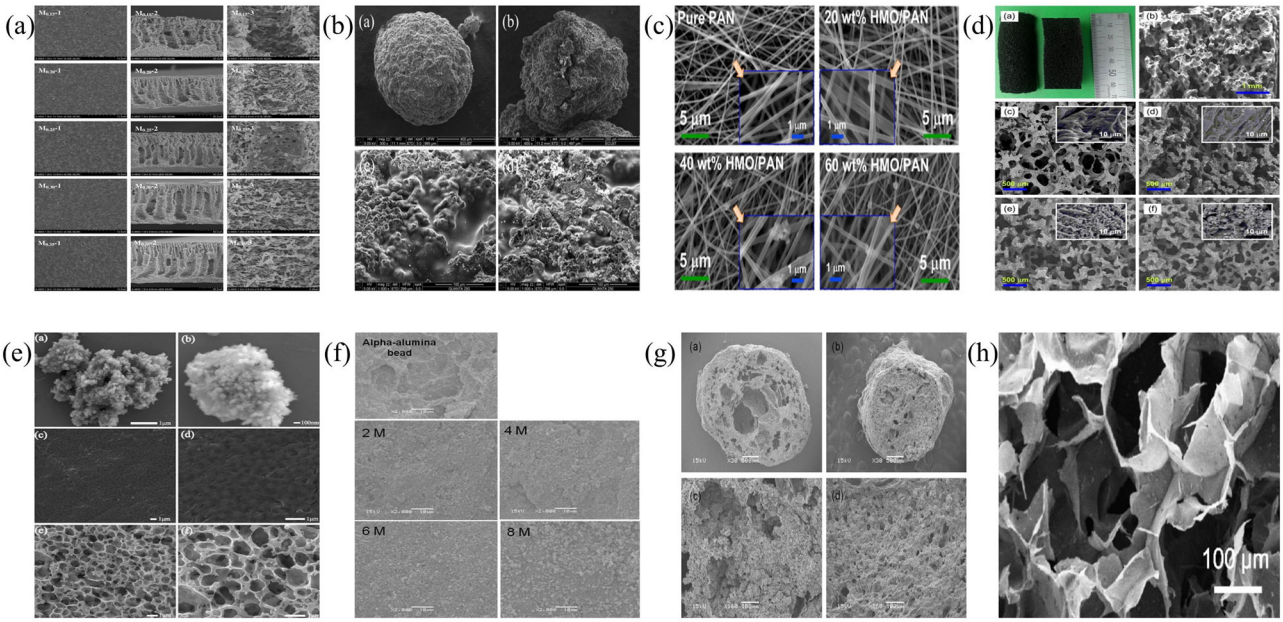

Fig. 14 | Morphological characterization of LMO composites. SEM images of **a** PVC-LMO membranes. Adapted from Zhu et al.[142]; **b** PAM-MnO_2 film. Adapted from Xiao et al.[143]; **c** Nanofiber-type PAN-LMO. Adapted from Park et al.[144]; **d** PVA-LMO foam. Adapted from Nisola et al.[145]; **e** PVDF-LMO composite. Adapted from Sun et al.[146]; **f** AAB-HMO. Adapted from Hong et al.[147]; **g** Chitosan-LMO. Adapted from Hong et al.[147]; **h** Cellulose-HMO film. Reprinted (adapted) with permission from Tang et al.[149].

factor (α) of 4.76 with respect to Mg^{2+}[146]. Hong et al. developed alpha-alumina beads (AAB) immobilized with HMO (Fig. 14f), which demonstrated a Li uptake capacity of 8.87 mg·g^{-1} in real seawater, surpassing HMO powder due to improved seawater contact[147]. In another study, Hong et al. synthesized chitosan-LMO (Fig. 14g) granules with mesoporous structures (pore sizes 6.5 to 30 nm), achieving a Li adsorption capacity of 11.4 mg·g^{-1}, comparable to LMO powder[148]. Finally, Tang et al. prepared a cellulose-HMO film (Fig. 14h) that exhibited remarkable selectivity for Li in seawater, extracting 99% of the Li^+ while maintaining less than 4% extraction for other ions like Sr^{2+}, K^+ and Ca^{2+}[149]. The cellulose-HMO film showed stable Li uptake capacity and mechanical strength over eight adsorption–desorption cycles.

Currently, the application of LMO composite materials is largely limited to laboratory-scale experiments. However, the results indicate that these materials hold substantial promises for scaling up Li extraction from brines. To advance this potential, future research should prioritize optimizing the performance and durability of LMO composites under real-world conditions, including testing with actual brines. Additionally, efforts should be directed towards developing scalable production processes to facilitate the transition from laboratory to industrial applications.

Conclusion

DLE presents a promising solution to meet the growing demand for Li, a key component in the production of batteries for electric vehicles and energy storage systems. This innovative approach involves extracting Li directly from brine resources, including unconventional sources like geothermal, oilfield brines, and even wastewater. DLE technologies offer several advantages over traditional extraction methods, including higher efficiency, reduced environmental impact, and faster processing times, which contribute to a more sustainable transition to clean energy. Among DLE technologies, ion exchange materials like LMOs stand out as one of the most promising candidates due to their high Li uptake capacities and rapid Li recovery kinetics. However, a significant challenge with LMO is Mn loss during the extraction process, which limits its practical application. To mitigate this issue, two strategies – doping and coating – are being explored to enhance the stability of LMOs. Additionally, LMO composite materials hold considerable potential for large-scale commercial DLE applications, offering a pathway to more efficient and sustainable Li extraction.

The scaling up of DLE technologies that use LMO materials faces several challenges, including material stability, scalability of LMO manufacturing, and uncertainties regarding their performance under varying conditions. To address these issues, future research and development efforts

must focus on optimizing LMO materials and enhancing their suitability for widespread, large-scale implementation. Although doping and coating have been proposed as potential solutions to mitigate Mn loss and enhance stability, identifying the appropriate materials and processes for these treatments at an industrial scale remains a significant hurdle. Importantly, these techniques must be fine-tuned to enhance LMO efficiency without introducing excessive complexity or cost to the production process. Furthermore, scaling up LMO and its composite materials for commercial use requires the development of robust and scalable manufacturing processes that ensure consistent material quality, high yields, and the ability to produce sufficient quantities to meet industrial-scale demand.

Further advancements in understanding LMO's behavior at the atomic level, through techniques like synchrotron-based X-ray absorption spectroscopy, will provide valuable insights into improving the chemistry and structural integrity of LMOs. Advances in LMO durability and resistance to harsh extraction conditions will be critical for achieving reliable and cost-effective operations. Enhancing the performance of LMO materials in various brine environments and scaling up the DLE processes to handle larger volumes are also key steps towards achieving cost-effective commercialization.

Data availability

No datasets were generated or analysed during the current study.

Received: 11 October 2024; Accepted: 19 June 2025;
Published online: 16 September 2025

References

1. Meng, F., McNeice, J., Zadeh, S. S. & Ghahreman, A. Review of Lithium Production and Recovery from Minerals, Brines, and Lithium-Ion Batteries. *Min. Proc. Ext. Met. Rev.* **42**, 123–141 (2019).
2. U.S. Geological Survey. *Mineral Commodity Summaries 2025*. https://doi.org/10.3133/mcs2025 (2025).
3. Murphy, O. & Haji, M. N. A review of technologies for direct lithium extraction from low Li^+ concentration aqueous solutions. *Front. Chem. Eng.* **4**, 1008680 (2022).
4. Fleischmann, J. et al. Battery 2030: Resilient, sustainable, and circular. McKinsey & Company https://www.mckinsey.com/industries/automotive-and-assembly/our-insights/battery-2030-resilient-sustainable-and-circular (2023).
5. Kaunda, R. B. Potential environmental impacts of lithium mining. *J. Energy Nat. Resour. Law* **38**, 237–244 (2020).
6. U.S. Geological Survey. *Mineral Commodity Summaries 2024*. https://doi.org/10.3133/mcs2024 (2024).
7. Stampatori, D., Raimondi, P. P. & Noussan, M. Li-ion batteries: A review of a key technology for transport decarbonization. *Energies* **13**, 2638 (2020).
8. Althaf, S. & Babbitt, C. W. Disruption risks to material supply chains in the electronics sector. *Resour. Conserv. Recycl.* **167**, 105248 (2021).
9. Xie, R. et al. Review of the research on the development and utilization of clay-type lithium resources. *Particuology* **87**, 46–53 (2024).
10. Swain, B. Recovery and recycling of lithium: A review. *Sep. Purif. Technol.* **172**, 388–403 (2017).
11. Li, X. et al. Membrane-based technologies for lithium recovery from water lithium resources: A review. *J. Membr. Sci.* **591**, 117317 (2019).
12. Zavahir, S. et al. A review on lithium recovery using electrochemical capturing systems. *Desalination* **500**, 114883 (2021).
13. Tran, T. & Luong, V. T. Lithium Production Processes. in *Lithium Process Chemistry: Resources, Extraction, Batteries, and Recycling* 81–124 (Elsevier Inc., 2015).
14. Tabelin, C. B. et al. Towards a low-carbon society: A review of lithium resource availability, challenges and innovations in mining, extraction and recycling, and future perspectives. *Miner. Eng.* **163**, 106743 (2021).
15. Flexer, V., Baspineiro, C. F. & Galli, C. I. Lithium recovery from brines: A vital raw material for green energies with a potential environmental impact in its mining and processing. *Sci. Total Environ.* **639**, 1188–1204 (2018).
16. Stringfellow, W. T. & Dobson, P. F. Technology for the Recovery of Lithium from Geothermal Brines. *Energies* **14**, 6805 (2021).
17. Grosjean, C., Miranda, P. H., Perrin, M. & Poggi, P. Assessment of world lithium resources and consequences of their geographic distribution on the expected development of the electric vehicle industry. *Renew. Sustain. Energy Rev.* **16**, 1735–1744 (2012).
18. Reich, R., Slunitschek, K., Danisi, R. M., Eiche, E. & Kolb, J. Lithium Extraction Techniques and the Application Potential of Different Sorbents for Lithium Recovery from Brines. *Min. Proc. Ext. Met. Rev.* **44**, 261–280 (2022).
19. Tadesse, B., Makuei, F., Albijanic, B. & Dyer, L. The beneficiation of lithium minerals from hard rock ores: A review. *Miner. Eng.* **131**, 170–184 (2019).
20. Vikström, H., Davidsson, S. & Höök, M. Lithium availability and future production outlooks. *Appl. Energy* **110**, 252–266 (2013).
21. Chandrasekharam, D. et al. Lithium: An energy transition element, its role in the future energy demand and carbon emissions mitigation strategy. *Geothermics* **119**, 102959 (2024).
22. Comboni, D. et al. High-pressure behavior and phase transition of jadarite, a promising B and Li mineral commodity. *J. Am. Ceram. Soc.* **105**, 7011–7021 (2022).
23. Gourcerol, B., Gloaguen, E., Melleton, J., Tuduri, J. & Galiegue, X. Re-assessing the European lithium resource potential – A review of hard-rock resources and metallogeny. *Ore Geol. Rev.* **109**, 494–519 (2019).
24. Zhu, L., Gu, H., Wen, H. & Yang, Y. Lithium extraction from clay-type lithium resource using ferric sulfate solutions via an ion-exchange leaching process. *Hydrometallurgy* **206**, 105759 (2021).
25. Dugamin, E. J. M. et al. Groundwater in sedimentary basins as potential lithium resource: a global prospective study. *Sci. Rep.* **11**, 21091 (2021).
26. Zhang, Y., Hu, Y., Wang, L. & Sun, W. Systematic review of lithium extraction from salt-lake brines via precipitation approaches. *Min. Eng.* **139**, 105868 (2019).
27. Roy Eccles, D. & Michael Dufresne, Pg. B. *Partb Nts 83k Assessment Report For 2016 Exploration On The Fox Creek Lithium-Brine Project*, *West-Central Alberta*. (2017).
28. Seip, A. et al. Lithium recovery from hydraulic fracturing flowback and produced water using a selective ion exchange sorbent. *Chem. Eng. J.* **426**, 130713 (2021).
29. Chen, Q. B. et al. Development of recovering lithium from brines by selective-electrodialysis: Effect of coexisting cations on the migration of lithium. *J. Memb. Sci.* **548**, 408–420 (2018).
30. Pramanik, B. K. et al. Lithium recovery from salt-lake brine: Impact of competing cations, pretreatment and preconcentration. *Chemosphere* **260**, 127623 (2020).
31. An, J. W. et al. Recovery of lithium from Uyuni salar brine. *Hydrometallurgy* **117–118**, 64–70 (2012).
32. Hwang, F. S. et al. Review of battery thermal management systems in electric vehicles. *Renew. Sustain. Energy Rev.* **192**, 114171 (2024).
33. Baum, Z. J., Bird, R. E., Yu, X. & Ma, J. Lithium-ion battery recycling—overview of techniques and trends. *ACS Energy Lett* **7**, 712–719 (2022).
34. Li, J., Li, L., Yang, R. & Jiao, J. Assessment of the lifecycle carbon emission and energy consumption of lithium-ion power batteries recycling: A systematic review and meta-analysis. *J. Energy Storage.* **65**, 107306 (2023).
35. Dalini, E. A., Karimi, G. H., Zandevakili, S. & Goodarzi, M. A review on environmental, economic and hydrometallurgical processes of

recycling spent lithium-ion batteries. *Min. Proc. Ext. Metall. Rev.* **42**, 451–472 (2020).
36. Meshram, P., Pandey, B. D. & Mankhand, T. R. Extraction of lithium from primary and secondary sources by pre-treatment, leaching and separation: A comprehensive review. *Hydrometallurgy* **150**, 192–208 (2014).
37. Knierim, K. J. et al. Evaluation of the lithium resource in the Smackover Formation brines of southern Arkansas using machine learning. *Sci. Adv.* **10**, eadp8149 (2024).
38. Benson, T. R., Coble, M. A. & Dilles, J. H. Hydrothermal enrichment of lithium in intracaldera illite-bearing claystones. *Sci. Adv.* **9**, eadh8183 (2023).
39. Lithium Americas. Lithium-Americas-Increases-Mineral-Resource-and-Reserve-for-Thacker-Pass-2025. (2025).
40. Core Lithium. *2024 Annual Report*. (2024).
41. Abbey, D., Sc, M., Geo, P., Haluszka, A. & Ehren, P. E3 Lithium 43-101 Technical Report: Lithium Resource EstimateBashaw District Project, Central Alberta. (2023).
42. Fosu, A. Y., Kanari, N., Vaughan, J. & Chagnes, A. Literature Review and Thermodynamic Modelling of Roasting Processes for Lithium Extraction from Spodumene. *Metals* **10**, 1312 (2020).
43. Nicolaci, H. et al. Global Metals & Mining Direct Lithium Extraction: A Potential Game Changing Technology. www.gs.com/research/hedge.html. (2023).
44. Ibarra-Gutiérrez, S., Bouchard, J., Laflamme, M. & Fytas, K. Project economics of lithium mines in Quebec: A critical review. *Extract. Ind. Soc.* **8**, 100984 (2021).
45. Mousavinezhad, S., Nili, S., Fahimi, A. & Vahidi, E. Environmental impact assessment of direct lithium extraction from brine resources: Global warming potential, land use, water consumption, and charting sustainable scenarios. *Resour. Conserv. Recycl.* **205**, 107583 (2024).
46. Festin, E. S., Tigabu, M., Chileshe, M. N., Syampungani, S. & Odén, P. C. Progresses in restoration of post-mining landscape in Africa. *J. For. Res.* **30**, 381–396 (2019).
47. Dordevic, D. et al. The influence of exploration activities of a potential lithium mine to the environment in Western Serbia. *Sci. Rep.* **14**, 17090 (2024).
48. Safari, S., Lottermoser, B. G. & Alessi, D. S. Metal oxide sorbents for the sustainable recovery of lithium from unconventional resources. *Appl. Mater. Today* **19**, 100638 (2020).
49. Vera, M. L., Torres, W. R., Galli, C. I., Chagnes, A. & Flexer, V. Environmental impact of direct lithium extraction from brines. *Nat. Rev. Earth Environ.* **4**, 149–165 (2023).
50. Baudino, L., Santos, C., Pirri, C. F., La Mantia, F. & Lamberti, A. Recent Advances in the Lithium Recovery from Water Resources: From Passive to Electrochemical Methods. *Adv. Sci.* **9**, 2201380 (2022).
51. Liu, D., Zhao, Z., Xu, W., Xiong, J. & He, L. A closed-loop process for selective lithium recovery from brines via electrochemical and precipitation. *Desalination* **519**, 115302 (2022).
52. Lima, M. C. C., Pontes, L. P., Vasconcelos, A. S. M., de Araujo Silva Junior, W. & Wu, K. Economic aspects for recycling of used lithium-ion batteries from electric vehicles. *Energies* **15**, 2203 (2022).
53. Hantanasirisakul, K. & Sawangphruk, M. Sustainable Reuse and Recycling of Spent Li-Ion batteries from Electric Vehicles: Chemical, Environmental, and Economical Perspectives. *Glob. Chall.* **7**, 2200212 (2023).
54. Chen, Q. et al. Evaluating environmental impacts of different hydrometallurgical recycling technologies of the retired nickel-manganese-cobalt batteries from electric vehicles in China. *Sep. Purif. Technol.* **311**, 123277 (2023).
55. Dunn, J. B., Gaines, L., Sullivan, J. & Wang, M. Q. Impact of recycling on cradle-to-gate energy consumption and greenhouse gas emissions of automotive lithium-ion batteries. *Environ. Sci. Technol.* **46**, 12704–12710 (2012).
56. Sun, Y., Wang, Q., Wang, Y., Yun, R. & Xiang, X. Recent advances in magnesium/lithium separation and lithium extraction technologies from salt lake brine. *Sep. Purif. Technol.* **256**, 117807 (2021).
57. Chen, J. & Wu, Z. Solvation extraction by amines and synergistic solvation extraction with neutral or acidic extractants. *Miner. Process. Extract. Metall. Rev.* **21**, 49–87 (2000).
58. Hanada, T. & Goto, M. Synergistic deep eutectic solvents for lithium extraction. *ACS Sustain Chem. Eng* **9**, 2152–2160 (2021).
59. Raiguel, S., Van Bogaert, L., Balcaen, T. & Binnemans, K. Selective extraction of lithium over alkali and alkaline earth ions by synergistic solvent extraction. *Green Chem* **27**, 1194–1205 (2024).
60. Azevedo, M. et al. *Lithium mining: How new production technologies could fuel the global EV revolution*. (McKinsey & Company, 2022).
61. Warren, I. *Techno-Economic Analysis of Lithium Extraction from Geothermal Brines*. https://doi.org/10.2172/1782801 (2021).
62. Xu, P., Hong, J. & Qian, X. et al. Materials for lithium recovery from salt lake brine. *J. Mater. Sci.* **56**, 16–63 (2021).
63. Khalil, A., Mohammed, S., Hashaikeh, R. & Hilal, N. Lithium recovery from brine: Recent developments and challenges. *Desalination* **528**, 115611 (2022).
64. Zhang, Y.-N. et al. Advances and promotion strategies of membrane-based methods for extracting lithium from brine. *Desalination* **566**, 116891 (2023).
65. Kowacz, M. & Pollack, G. H. Cells in new light: Ion concentration, voltage, and pressure gradients across a hydrogel membrane. *ACS Omega* **5**, 21024–21031 (2020).
66. Wang, L. et al. Salt and water transport in reverse osmosis membranes: beyond the solution-diffusion model. *Environ. Sci. Technol.* **55**, 16665–16675 (2021).
67. Chitrakar, R., Makita, Y., Ooi, K. & Sonoda, A. Magnesium-doped manganese oxide with lithium ion-sieve property: Lithium adsorption from salt lake brine. *Bull. Chem. Soc. Jpn* **86**, 850–855 (2013).
68. Xu, F., Dai, L., Wu, Y. & Xu, Z. Li^+/Mg^{2+} separation by membrane separation: The role of the compensatory effect. *J. Memb. Sci.* **636**, 119542 (2021).
69. Zhang, T., Zheng, W., Wang, Q., Wu, Z. & Wang, Z. Designed strategies of nanofiltration technology for Mg^{2+}/Li^+ separation from salt-lake brine: A comprehensive review. *Desalination* **546**, 116205 (2023).
70. Fan, F. et al. A Bioinspired Membrane with Ultrahigh Li^+/Na^+ and Li^+/K^+ Separations Enables Direct Lithium Extraction from Brine. *Adv. Sci.* **11**, 2402898 (2024).
71. Farahbakhsh, J. et al. Direct lithium extraction: A new paradigm for lithium production and resource utilization. *Desalination* **575**, 117249 (2024).
72. Somrani, A., Hamzaoui, A. H. & Pontie, M. Study on lithium separation from salt lake brines by nanofiltration (NF) and low pressure reverse osmosis (LPRO). *Desalination* **317**, 184–192 (2013).
73. Zhao, Z., Si, X., Liu, X., He, L. & Liang, X. Li extraction from high Mg/Li ratio brine with $LiFePO_4/FePO_4$ as electrode materials. *Hydrometallurgy* **133**, 75–83 (2013).
74. Liu, X., Chen, X., He, L. & Zhao, Z. Study on extraction of lithium from salt lake brine by membrane electrolysis. *Desalination* **376**, 35–40 (2015).
75. Xu, W., He, L. & Zhao, Z. Lithium extraction from high Mg/Li brine via electrochemical intercalation/de-intercalation system using LiMn2O4 materials. *Desalination* **503**, 114935 (2021).
76. Liu, C. et al. Lithium Extraction from Seawater through Pulsed Electrochemical Intercalation. *Joule* **4**, 1459–1469 (2020).

77. Sun, S. et al. Green recovery of lithium from geothermal water based on a novel lithium iron phosphate electrochemical technique. *J. Clean. Prod.* **247**, 119178 (2020).
78. Wang, J. & Koenig, G. M. Direct lithium extraction using int ercalation materials. *Chem. Eur. J*. **30**, (2023).
79. Guo, Z. Y. et al. Effect of impurity ions in the electrosorption lithium extraction process: generation and restriction of 'Selective Concentration Polarization'. *ACS Sustain. Chem. Eng.* **8**, 11834–11844 (2020).
80. Kong, L. et al. Electro-driven direct lithium extraction from geothermal brines to generate battery-grade lithium hydroxide. *Nat. Commun.* **16**, 806 (2025).
81. Freiderich, J. W. Low temperature lithium production of lithium. *US 10,718,057 B1* (2020).
82. Bernini, F. et al. Water-assisted electrosynthesis of a lithium–aluminum intermetallic from a lithium chloride-ionic liquid melt. *ACS Electrochem.* **1**, 599–606 (2025).
83. Lin, S. et al. Double-edged role of interlayer water on Li^+ extraction from ultrahigh Mg^{2+}/Li^+ ratio brines using Li/Al-LDHs. *J. Colloid Interface Sci*. **627**, 872–879 (2022).
84. Paranthaman, M. P. et al. Recovery of lithium from geothermal brine with lithium-aluminum layered double hydroxide chloride sorbents. *Environ. Sci. Technol.* **51**, 13481–13486 (2017).
85. Jiang, H., Yang, Y., Sun, S. & Yu, J. Adsorption of lithium ions on lithium-aluminum hydroxides: Equilibrium and kinetics. *Can. J. Chem. Eng.* **98**, 544–555 (2020).
86. Li, Y. et al. Performance activation mechanism of aluminum-based layered double hydroxides adsorbents for recovering Li^+ by pH modulating. *Chem. Eng. J.* **494**, 152919 (2024).
87. Lv, S. et al. Anion regulation strategy of lithium-aluminum layered double hydroxides for strengthening resistance to deactivation in lithium recovery from brines. *Chem. Eng. J.* **472**, 145026 (2023).
88. Pan, Y. et al. Selective extraction of lithium from shale gas produced water using an aluminum-based adsorbent. *Green. Smart Min. Eng.* **1**, 208–219 (2024).
89. Xu, N. et al. Synthesis of $H_4Mn_5O_{12}$ Nanotubes lithium ion sieve and its adsorption properties for Li^+ from aqueous solution. *ChemistrySelect* **4**, 9562–9569 (2019).
90. Zhang, J., Gao, Q., Han, B. & Zhou, C. Mechanism of lithium ion selectivity through membranes: a brief review. *Environ. Sci.-Water Res. Tech.* **10**, 1305–1318 (2024).
91. Zhang, Q. H., Li, S. P., Sun, S. Y., Yin, X. S. & Yu, J. G. $LiMn_2O_4$ spinel direct synthesis and lithium ion selective adsorption. *Chem. Eng. Sci.* **65**, 169–173 (2010).
92. Zhang, Q. H., Sun, S., Li, S., Jiang, H. & Yu, J. G. Adsorption of lithium ions on novel nanocrystal MnO_2. *Chem. Eng. Sci.* **62**, 4869–4874 (2007).
93. Sun, J. et al. Preparation of high hydrophilic H_2TiO_3 ion sieve for lithium recovery from liquid lithium resources. *Chem. Eng. J.* **453**, 139485 (2023).
94. Weng, D. et al. Introduction of manganese based lithium-ion Sieve-A review. *Prog. Nat. Sci. Mater. Int.* **30**, 139–152 (2020).
95. Xu, X. et al. Extraction of lithium with functionalized lithium ion-sieves. *Prog. Mater. Sci.* **84**, 276–313 (2016).
96. Ceder, G., Van Der Ven, A., Marianetti, C. & Morgan, D. First-principles alloy theory in oxides. *Model. Simul. Mater. Sci. Eng.* **8**, 311–321 (2000).
97. Zhang, S. et al. Mitigating the Jahn-Teller distortion driven by the spin-orbit coupling of lithium manganate cathode. *J. Energy Chem.* **72**, 379–387 (2022).
98. Liu, T. et al. Correlation between manganese dissolution and dynamic phase stability in spinel-based lithium-ion battery. *Nat. Commun.* **10**, 4721 (2019).
99. Xiao, G. et al. Adsorption and desorption behavior of lithium ion in spherical PVC-MnO_2 ion sieve. *Ind. Eng. Chem. Res.* **51**, 10921–10929 (2012).
100. Liu, W.-X. et al. Nanomaterials with Excellent Adsorption Characteristics for Sample Pretreatment: A Review. *Nanomaterials* **12**, 1845 (2022).
101. Xu, J., Wei, X., Han, J. & Qin, W. Synthesis and optimisation mechanism of functionalised adsorption materials for lithium-ion extraction from salt water: A review. *Sep. Purif. Technol.* **339**, 126237 (2024).
102. Ding, W. et al. Synthesis of granulated $H_4Mn_5O_{12}$/chitosan with improved stability by a novel cross-linking strategy for lithium adsorption from aqueous solutions. *Chem. Eng. J.* **426**, 131689 (2021).
103. Wang, L., Ma, W., Liu, R., Li, H. Y. & Meng, C. G. Correlation between Li^+ adsorption capacity and the preparation conditions of spinel lithium manganese precursor. *Solid State Ion.* **177**, 1421–1428 (2006).
104. Chitrakar, R., Kanoh, H., Miyai, Y. & Ooi, K. Recovery of lithium from seawater using manganese oxide adsorbent ($H_{1.6}Mn_{1.6}O_4$) derived from $Li_{1.6}Mn_{1.6}O_4$. *Ind. Eng. Chem. Res.* **40**, 2054–2058 (2001).
105. Shi, X. et al. Synthesis and properties of $Li_{1.6}Mn_{1.6}O_4$ and its adsorption application. *Hydrometallurgy* **110**, 99–106 (2011).
106. Zandevakili, S., Ranjbar, M. & Ehteshamzadeh, M. Recovery of lithium from Urmia Lake by a nanostructure MnO_2 ion sieve. *Hydrometallurgy* **149**, 148–152 (2014).
107. Chitrakar, R., Makita, Y., Ooi, K. & Sonoda, A. Selective uptake of lithium ion from brine by $H_{1.33}Mn_{1.67}O_4$ and $H_{1.6}Mn_{1.6}O_4$. *Chem. Lett.* **41**, 1647–1649 (2012).
108. Yu, Y., Guo, Y., Ning, P. & Aziguli, H. A Mg^{2+}/Al^{3+} dual-doped $LiMn_2O_4$ as high-performance cathode material for high-rate and long-cycle lithium-ion batteries. *J. Energy Storage* **110**, 115309 (2025).
109. Marincaş, A.-H. & Ilea, P. Enhancing lithium manganese oxide electrochemical behavior by doping and surface modifications. *Coatings* **11**, 456 (2021).
110. Xiong, L., Xu, Y., Zhang, C., Zhang, Z. & Li, J. Electrochemical properties of tetravalent Ti-doped spinel $LiMn_2O_4$. *J. Solid State Electrochem* **15**, 1263–1269 (2011).
111. Bohnke, O., Bohnke, C. & Fourquet, J. L. Mechanism of ionic conduction and electrochemical intercalation of lithium into the perovskite lanthanum lithium titanate. *Solid State Ionics* **91**, 21–31 (1996).
112. Martínez-Juárez, A., Pecharromán, C., Iglesias, J. E. & Rojo, J. M. Relationship between Activation Energy and Bottleneck Size for Li^+ Ion Conduction in NASICON Materials of Composition $LiMM'(PO_4)_3$; M, M' = Ge, Ti, Sn, Hf. *J. Phys. Chem. B* **102**, 372–375 (1998).
113. Katsumata, T., Matsui, Y., Inaguma, Y. & Itoh, M. Influence of site percolation and local distortion on lithium ion conductivity in perovskite-type oxides $La_{0.55}Li_{0.35-x}K_xTiO3$ and $La_{0.55}Li_{0.35}TiO_3$-KMO_3 (M = Nb and Ta). *Solid State Ion.* **86–88**, 165–169 (1996).
114. Dean, J. A. & Lange, N. Adolph. *Lange's Handbook of Chemistry*. (McGraw-Hill; [Distributed by] Knovel, 2001).
115. Qian, F. et al. Surface trace doping of Na enhancing structure stability and adsorption properties of $Li_{1.6}Mn_{1.6}O_4$ for Li^+ recovery. *Sep. Purif. Technol.* **256**, 117583 (2021).
116. Qian, F. et al. K-gradient doping to stabilize the spinel structure of $Li_{1.6}Mn_{1.6}O_4$for Li^+ recovery. *Dalton Trans.* **49**, 10939–10948 (2020).
117. Bao, L. et al. Preparation of Mg-doped $Li_{1.6}Mn_{1.6}O_4$ with enhanced Li^+ adsorption performance and anti-dissolution properties of Mn. *Hydrometallurgy* **209**, 105772 (2022).
118. Qian, F. et al. Enhancing the Li^+ adsorption and anti-dissolution properties of $Li_{1.6}Mn_{1.6}O_4$ with Fe, Co doped. *Hydrometallurgy* **193**, 105291 (2020).

119. Zhang, G. et al. Synthesis of aluminum-doped ion-sieve manganese oxides powders with enhanced adsorption performance. *Colloids Surf A Physicochem. Eng. Asp*. **583**, 123950 (2019).
120. Cao, G. et al. Synthesis, adsorption properties and stability of Cr-doped lithium ion sieve in Salt Lake Brine. *Bull. Chem. Soc. Jpn* **92**, 1205–1210 (2019).
121. Chitrakar, R., Makita, Y., Ooi, K. & Sonoda, A. Synthesis of iron-doped manganese oxides with an ion-sieve property: Lithium adsorption from bolivian brine. *Ind. Eng. Chem. Res.* **53**, 3682–3688 (2014).
122. Ju, S., Xue, F., Qian, J., Chen, F. & Wang, B. Synthesis of Ga^{3+} doped lithium manganese ion sieve for Li^+ extraction and its adsorption thermodynamic behavior. *Sep Sci. Technol.* **57**, 2923–2936 (2022).
123. Ryu, T. et al. Mechanochemical synthesis of silica-lithium manganese oxide composite for the efficient recovery of lithium ions from seawater. *Solid State Ion* **308**, 77–83 (2017).
124. Ryu, T., Shin, J., Ghoreishian, S. M., Chung, K. S. & Huh, Y. S. Recovery of lithium in seawater using a titanium intercalated lithium manganese oxide composite. *Hydrometallurgy* **184**, 22–28 (2019).
125. Herrmann, L. et al. Lithium recovery from geothermal brine - an investigation into the desorption of lithium ions using manganese oxide adsorbents. *Energy Adv*. 877–885 (2022)
126. Ooi, K. et al. Recovery of lithium from salt-brine eluates by direct crystallization as lithium sulfate. *Hydrometallurgy* **174**, 123–130 (2017).
127. Xu, S. et al. Lithium transport through lithium-ion battery cathode coatings. *J. Mater. Chem. A Mater.* **3**, 17248–17272 (2015).
128. Riyanto, E. et al. A review of atomic layer deposition for high lithium-ion battery performance. *J. Mater. Res. Technol.* **15**, 5466–5481 (2021).
129. Lu, Z., Hao, S., Aykol, M., Yao, Z. & Wolverton, C. Lithium Transport in crystalline and amorphous cathode coatings for Li-ion batteries. *Chem. Mater.* **36**, 10205–10215 (2024).
130. Nolan, A. M., Wickramaratne, D., Bernstein, N., Mo, Y. & Johannes, M. D. Li^+ diffusion in amorphous and crystalline Al_2O_3 for battery electrode coatings. *Chem. Mater.* **33**, 7795–7804 (2021).
131. Wang, L. et al. Synthesis of zirconium-coated lithium ion sieve with enhanced cycle stability. *Sep Purif. Technol.* **303**, 121933 (2022).
132. Ohashi, F. & Tai, Y. Lithium adsorption from natural brine using surface-modified manganese oxide adsorbents. *Mater. Lett.* **251**, 214–217 (2019).
133. Li, H. et al. Annealed SiO_2 Protective Layer on $LiMn_2O_4$ for Enhanced Li-Ion Extraction from Brine. *Nano Lett*. **23**, 10458–10465 (2023).
134. Somo, T. R. et al. A comparative review of metal oxide surface coatings on three families of cathode materials for lithium ion batteries. *Coatings* **11**, 744 (2021).
135. Qureshi, Z. A., Tariq, H. A., Shakoor, R. A., Kahraman, R. & AlQaradawi, S. Impact of coatings on the electrochemical performance of $LiNi_{0.5}Mn_{1.5}O_4$ cathode materials: A focused review. *Ceram. Int.* **48**, 7374–7392 (2022).
136. Guan, P. et al. Recent progress of surface coating on cathode materials for high-performance lithium-ion batteries. *J. Energy Chem.* **43**, 220–235 (2020).
137. Naghdi, S., Rhee, K. Y., Hui, D. & Park, S. J. A review of conductive metal nanomaterials as conductive, transparent, and flexible coatings, thin films, and conductive fillers: Different deposition methods and applications. *Coatings* **8**, 278 (2018).
138. Mavukkandy, M. O. et al. Thin film deposition techniques for polymeric membranes– A review. *J. Memb. Sci.* **610**, 118258 (2020).
139. Gao, Y. et al. Graphite recycling from the spent Lithium-ion batteries by sulfuric acid curing-leaching combined with high-temperature calcination. *ACS Sustain. Chem. Eng.* **8**, 9447–9455 (2020).
140. Ma, X., Chen, M., Chen, B., Meng, Z. & Wang, Y. High-performance graphite recovered from spent Lithium-ion batteries. *ACS Sustain Chem. Eng* **7**, 19732–19738 (2019).
141. Windisch-Kern, S. et al. Recycling chains for lithium-ion batteries: A critical examination of current challenges, opportunities and process dependencies. *Waste Manage*. **138**, 125–139 (2022).
142. Zhu, G., Wang, P., Qi, P. & Gao, C. Adsorption and desorption properties of Li^+ on PVC-$H_{1.6}Mn_{1.6}O_4$ lithium ion-sieve membrane. *Chem. Eng. J.* **235**, 340–348 (2014).
143. Xiao, J. L., Sun, S. Y., Song, X., Li, P. & Yu, J. G. Lithium ion recovery from brine using granulated polyacrylamide–MnO_2 ion-sieve. *Chem. Eng. J.* **279**, 659–666 (2015).
144. Park, M. J. et al. Recyclable composite nanofiber adsorbent for Li^+ recovery from seawater desalination retentate. *Chem. Eng. J.* **254**, 73–81 (2014).
145. Nisola, G. M. et al. Macroporous flexible polyvinyl alcohol lithium adsorbent foam composite prepared via surfactant blending and cryo-desiccation. *Chem. Eng. J.* **280**, 536–548 (2015).
146. Sun, D. et al. Highly selective, regenerated ion-sieve microfiltration porous membrane for targeted separation of Li^+. *J. Porous Mater.* **23**, 1411–1419 (2016).
147. Hong, H. J. et al. Immobilization of hydrogen manganese oxide (HMO) on alpha-alumina bead (AAB) to effective recovery of Li^+ from seawater. *Chem. Eng. J.* **271**, 71–78 (2015).
148. Hong, H. J. et al. Granulation of $Li_{1.33}Mn_{1.67}O_4$ (LMO) through the use of cross-linked chitosan for the effective recovery of Li^+ from seawater. *Chem. Eng. J.* **234**, 16–22 (2013).
149. Tang, L. et al. Highly efficient, stable, and recyclable hydrogen manganese oxide/cellulose film for the extraction of lithium from seawater. *ACS Appl Mater. Interfaces* **12**, 9775–9781 (2020).
150. Orooji, Y. et al. Recent advances in nanomaterial development for lithium ion-sieving technologies. *Desalination* **529**, 115624 (2022).
151. Berg, H., Göransson, K., Noläng, B. & Thomas, J. O. Electronic structure and stability of $Li_{1+x}Mn_{2-x}O_4$ spinels. *J. Mater. Chem.* **10**, 1437–1441 (2000).
152. Murodjon, S., Yu, X., Li, M., Duo, J. & Deng, T. Lithium Recovery from Brines Including Seawater, Salt Lake Brine, Underground Water and Geothermal Water. In *Thermodynamics and Energy Engineering* https://doi.org/10.5772/intechopen.90371 (IntechOpen, 2020)..
153. Boroumand, Y. & Razmjou, A. Adsorption-type aluminium-based direct lithium extraction: The effect of heat, salinity and lithium content. *Desalination* **577**, 117406 (2024).

Acknowledgements

The authors acknowledge funding from the Natural Sciences and Engineering Research Council of Canada (NSERC) Discovery program to DSA (RGPIN-2020-05289) and from the Future Energy Systems (FES T10-P06) research program, itself funded through a Canada First Research Excellence Fund (CFREF) award to the University of Alberta.

Author contributions

F.W. conducted the review and wrote the manuscript. K.R.S., K.O.K. and D.S.A. reviewed, edited, and formatted the manuscript. All authors conceptualized the review paper and read and approved the final manuscript.

Competing interests

D.S.A. is an Editorial Board Member of npj Materials Sustainability but is not involved in the peer-review process or decision making for this manuscript. All other authors declare no conflict of interest.

Additional information

Correspondence and requests for materials should be addressed to Daniel S. Alessi.